Ministry of Science and Higher Education of the Russian Federation
NATIONAL RESEARCH
TOMSK STATE UNIVERSITY (NR TSU)
Faculty of Physics
Department of General and Experimental Physics

ADMIT TO THE DEFENCE AT THE SEB

Director of the BEP
Doctor of Physics and Mathematics, Professor,
V.P. Demkin
17.06. 2019

MASTER'S THESIS

TECHNOLOGY OF EFFECTIVENESS IMPROVEMENT OF MRI DIAGNOSTICS OF TISSUE DISORDERS OF BLOOD SUPPLY IN THE INNER EAR

within the Basic Educational Programme of Master's Degree
subject area 03.04.02 – Physics

Viktor Yurjevich Babikov

Research supervisor
Dr., Professor
V.V. Udut
signature
14 июня 2019

Author
student of group No 536MB
V.Y. Babikov
signature

Tomsk
2019

NATIONAL RESEARCH
TOMSK STATE UNIVERSITY (NR TSU)
Faculty of Physics
Department of General and Experimental Physics

ASSIGNMENT
for preparing the Master's Thesis

Master's Student *Babikov Viktor Yurjevich*

(surname, name, patronymic, programme)

Basic Educational Programme of Master's Degree «Physics Methods and Information Technologies in Biomedicine», subject area 03.04.02 – Physics

Topic of the Master's Thesis *Technology of effectiveness improvement of MRI diagnostics of tissue disorders of blood supply in the inner ear*

Approved *Academic Council of the Faculty of Physics 26.10.2017№ 469*

Research Supervisor: *Udut Vladimir Vasilievich, Dr. of Med. Science, Professor*

(surname, name, patronymic, academic degree, title)

Terms of completion:

1) Preliminary plan and schedule for writing the Master's Thesis from

01 09 2018 to 01 10 2018.

2) Search and study of required legal documents, acts and special literature from

01 09 2018 to 20 04 2019.

3) Collection and analysis of practical material from 01 09 2018 to 20 04 2019.

Magnetic Resonance Imaging analysis of the blood supply of the inner ear with contrasting and changes in the rheological status of the blood. Vestibular system assessment using 1,5 Tesla, 3 Tesla MRI scanners without contrasting. Perfusion detection using Presto method (modified Echo Planar sequence).Processing of experimental data, analysis and comparison with literature (data).

4) Final plan of the Master's Thesis from 01 02 2019 to 15 02 2019.

5) Writing and formatting the Master's Thesis from 15 02 2019 to 10 06 2019.

6) Preparing and publishing an abstract of the Master's Thesis from 15 05 2019 to 10 06 2019.

7) Public presentation of the main ideas of the Master's Thesis/ participation in a planned research and scientific conference from 15 05 2019 to 06 06 2019.

8) Preparing a synopsis of the Master's Thesis from 15 05 2019 to 06 06 2019.

I declare that I have familiarised myself with the Guidelines for Preparing a FQP.

I further accept the assignment for execution

date and signature of the Master's Student

ABSTRACT

The temporal bone has a highly complex anatomical structure, in which the sensory organs of the cochlea and the vestibular system are contained within a small space together with the sound-conducting system of the middle ear. As known, the inner ear consists of cochlea, superior, posterior, horizontal canals, endolymphatic sac, saccule, utricle, Cochlea, ductus reuniens, utricular and sacullae maculae, crista ampullaris and fluids in the inner ear canals. Malformation of these compartments of inner ear can play tremendous role in the disease development such as Benign paroxysmal positional vertigo (bppv), ménière's disease, hearing loss [1, 2].

Structure of the fine osseous anatomy of the inner ear can be obtained using modern computed tomography (CT) scanners and cone beam CT (CBCT). Analysis of the soft-tissue constituents of the labyrinth, however, is beyond the scope of X-ray techniques. Both in the present and in the near future, anatomical structure of the membranous labyrinth can be expected from magnetic resonance imaging (MRI).

Tasks of the Master's thesis:

1. Anatomical structure of Vestibular system assessment using Magnetic Resonance Imaging 1,5 Tesla, 3Tesla.
2. Perfusion detecting using PRESTO method.

TABLE OF CONTENTS

LIST OF ABBREVIATIONS

CT	Computed tomography
CB CT	Cone beam computed tomography
MRI	Magnetic resonance imaging
MD	Meniere's disease
BPPV	Benign paroxysmal positional vertigo
HL	Hearing loss
UHF-MRI	Ultra- high field magnetic resonance imaging
DSC	Dynamic susceptibility contrast
DCE	Dynamic contrast enhancing
SV	Scala vestibuli
SM	Scala media
ST	Scala tympani
AICA	Anterior inferior cerebellar artery
VSBM	Vessel of the basilar membrane
VSTL	Vessel of the tympanic lip
VCAQ	Vein of the cochlear aqueduct
TE	Echo time
TR	Repetition time
RF	Radiofrequency
TOF	Time – of - flight
DWI	Diffusion weighted imaging
IR	Inversion recovery
FSE	Fast Spin Echo
MPrage	Magnetization-prepared 180 degrees radio-frequency pulses and rapid gradient-echo

DSC	Dynamic susceptibility contrasting
DCE	Dynamic contrast enhancement
ASL	Arterial Spin Labelling
GRE (GE)	Gradient echo
EPI	Echo planar imaging
SE	Spin echo
AIF	Acquisition related factors
PCASL	Pseudo-continuous arterial spinning labelling
CASL	Continuous Arterial Spin labeling
PLD	post-label delay
ATT	Arterial transit time
GRASE	Gradient and spin echo
ES	Echo shifting
ES-Flash	Echo shiting fast low angle shot magnetic resonance imaging
fMRI	Functional magnetic resonance imaging
PRESTO	Principles of echo-shifting with a train of observation
ARHL	Age related hearing loss
ES	Endolymphatic sac

INTRODUCTION

The temporal bone has a highly complex anatomical structure, in which the sensory organs of the cochlea and the vestibular system are contained within a small space together with the sound-conducting system of the middle ear. As known, the inner ear consists of cochlea, superior, posterior, horizontal canals, endolymphatic sac, saccule, utricle, Cochlea, ductus reuniens, utricular and sacullae maculae, crista ampullaris and fluids in the inner ear canals. Malformation of these compartments of inner ear can play tremendous role in the disease development such as Benign paroxysmal positional vertigo (bppv), ménière's disease, hearing loss [1, 13, 32].

Fluid disturbances in the inner ear represent a special medical challenge to otolaryngology and oto-neurology. The two inner ear fluids, perilymph and endolymph, play a critical role in inner ear homeostasis, and anomalies in the compartments containing these fluids may be associated with auditory neuropathy, acute peripheral vestibulopathy, neurovascular cross-compression, and endolymphatic hydrops or Meniere's disease. Moreover, the inner ear has a complex system of blood flow. It is principally supplied from the inner ear artery (labyrinthine artery), which is usually a branch of the anterior inferior cerebellar artery. Cochlear blood flow is a function of cochlear perfusion pressure, which is calculated as the difference between mean arterial blood pressure and inner ear fluid pressure. Thereby, impaired blood flow and malformations of endolymph and perilymph fluids make an additional contribution to diseases development. The human vestibular system is not easily accessible for investigation because this delicate sensory organ is hidden deep in the temporal bone [2, 3].

Understanding the parameters of blood flow, homeostasis and building a detailed anatomical structure of inner ear is a key to success in developing targeted pharmacological and surgery invasions in order to eliminate the diseases [3, 4].

Structure of the fine osseous anatomy of the inner ear can be obtained using modern computed tomography (CT) scanners and cone beam CT (CBCT). Analysis of the soft-tissue constituents of the labyrinth, however, is beyond the scope of X-ray techniques. Both in the present and in the near future, anatomical structure of the membranous labyrinth can (at best) be expected from magnetic resonance imaging (MRI). Contrast-enhanced magnetic resonance imaging (MRI) has become a frequently used clinical tool for diagnosis and examination of pathophysiology of inner ear and retrocochlear abnormalities. Currently, anatomical structure of the membranous labyrinth in the clinical setting remains a challenge despite significant technological advances [1 ,4, 13].

Despite tremendous advances in magnetic resonance imaging protocols in recent years, the ability to image finer details of membranous anatomy of the inner ear still lies in the domain of ul-

tra-high-field magnetic resonance imaging (UHF-MRI) scanners, defined here by a field strength equal to or greater than 7 T. Detailed clinical imaging of membranous components of the inner ear remains elusive because of the inability standard programs of commonly-available 3 T scanners to image the inner ear at adequate resolutions.

Several MRI research centers have attempted to visualize inner ear anatomy at 7 T, with varying degree of success. Structures such as the osseous spiral lamina and the labyrinthine artery can be visualized at 7 T, but the scala media and its boundary structures are indistinct or blurry at this field strength. The anatomy of the otoliths has been studied, but there is limited information regarding their supporting connective tissue structures such as the membrana limitans in humans [4, 5].

Therefore, It's remain unsolved problem for a medical community and detailed understanding of the deep relations of the footplate is crucial to assess the risks and outcomes of different intervention [15].

For this reason, the size baselines of inner ear compartments will be collected using MRI in our study. Moreover, we will try to detect perfusion of inner ear. If the result is success, in next studies, malformations of the inner compartments will be assessed and the blood flow, blood flow volume will be counted.

Tasks of the Master's thesis:

1. Anatomical structure of Vestibular system assessment using Magnetic Resonance Imaging 1,5 Tesla, 3Tesla and 7Tesla with the preliminary injecting of gadolininium-containing contrast agent – Gadovist.
2. Scanning performing of anatomical structure performing: Anatomical structures of Vestibule, Cochlea, Semicircular canals, endolymph and perilymph shaping using 1,5Tesla, 3Tesla and 7Tesla MRI.
3. Blood flow of vestibular system assessment using DSC and DSE of MRI specific methods.

1 Anatomical and physiological properties of the inner ear

1.1 Anatomical structure of inner ear

The inner ear contains the neurosensory organs of hearing and equilibrium, receiving the terminal distributions of the auditory and vestibular nerves. It is known as the labyrinth, because of the complexity of its shape and consists of 2 parts: the osseous labyrinth, the cavity within the petrous bone, and the membranous labyrinth, a series of communicating membranous sacs and ducts contained by the osseous cavity (Figure 1).

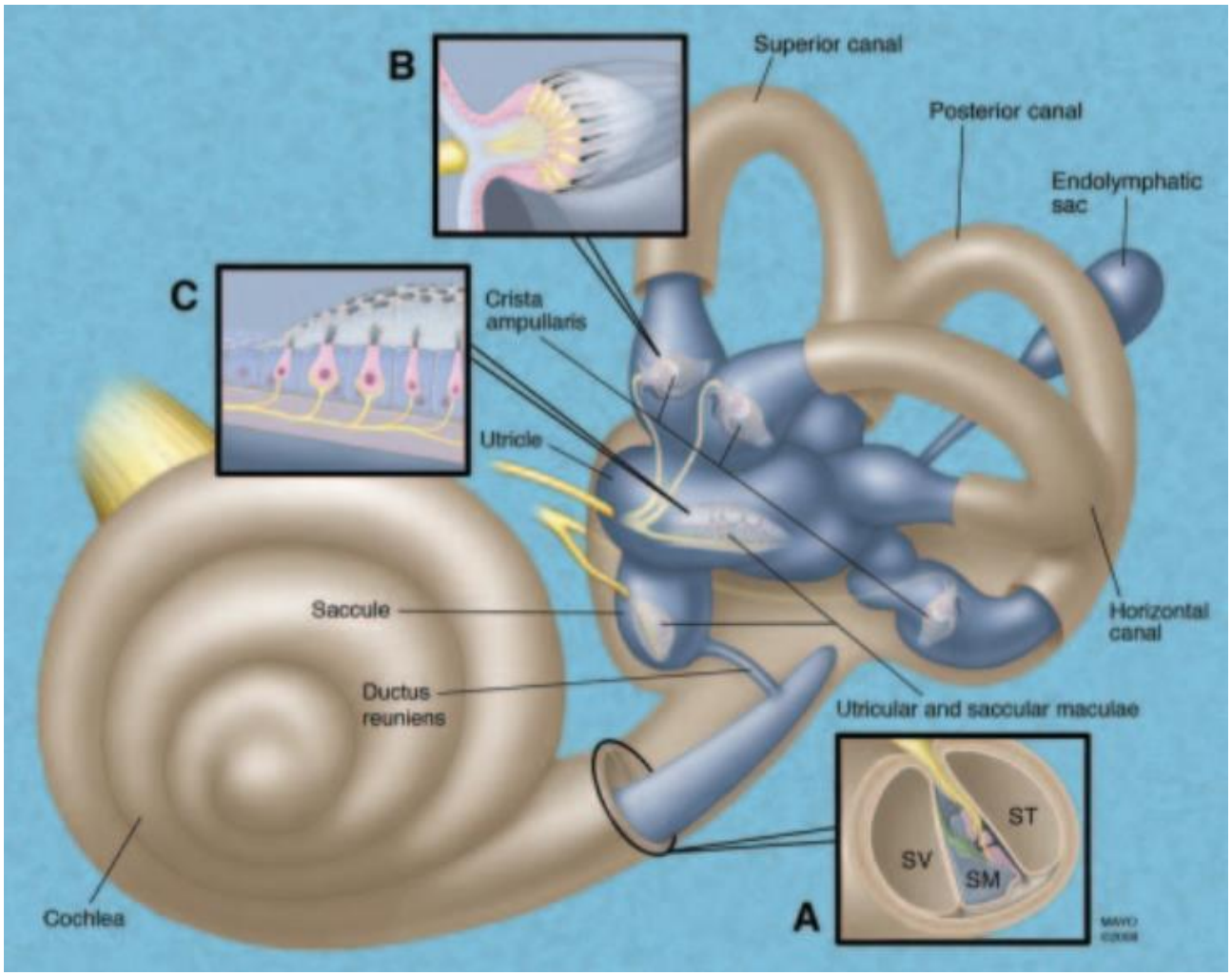

A – cross-section of the cochlea; B – view of the crista ampullaris of the superior semicircular duct; C – view of the utricular macula. SV indicates scala vestibuli; SM, scala media; ST, scala tympani.

Figure 1 – The anatomical structure of the inner ear and the membranous labyrinth

The membranous labyrinth is partly separated from the bony walls by the perilymph. The sacs and ducts of the membranous labyrinth are filled with endolymph, and branches of the acoustic and vestibular nerves terminate within the sensory epithelium of these endolymphatic vesicles. The

membranous structures of the bony vestibule do not quite preserve the form of the osseous cavity that contains them but consist of 2 membranous sacs, the utricle and the saccule. These structures contain the sensory organs that detect linear acceleration. The anterior floor of the utricle is focally thickened, consisting of thousands of otoliths floating on a gelatinous membrane beneath the neurosensory hair cells, which receive the utricular filaments of the superior vestibular nerve. This thickened area is the utricular macula. The cavity of the utricle communicates with the semicircular ducts by 5 orifices. It also communicates with the endolymphatic duct and saccule by way of the utriculo saccular duct. The saccule is the smaller of the 2 vestibular sacs and lies in the spherical recess of the medial wall of the bony vestibule near the opening of the scala vestibuli of the cochlea. The medial wall of the saccule exhibits an ellipsoid thickening, the saccular macula (identical in composition to the utricular macula), innervated by the saccular branch of the inferior vestibular nerve andoriented approximately 90°totheplane of the utricular macula. The endolymphatic duct, arising from the posterior wall of the saccule, joins the utriculo saccular duct and passes through the vestibular aqueduct to end in the endolymphatic sac on the posterior surface of the petrous bone, beneath the dura mater. The ductus reuniens arises from the floor of the saccule and opens into the cochlear duct near its vestibular end. The semicircular ducts occupy approximately one fourth of the cross-sectional area of the osseous canals but are of similar form, each with an ampullated end. They open by 5 orifices into the utricle, 1 opening being common to the posterior end of the superior duct and the superior end of the posterior duct (the common crus). In the ampullae, the wall is thickened, containing a fiddle-shaped transversely oriented complex of hair cells, the crista ampullaris. These sensory organs detect angular (ie, rotational) acceleration. The superior and horizontal ampullae are innervated by the superior vestibular nerve, and the posterior ampulla is innervated by the posterior (singular) branch of the inferior vestibular nerve. The utricle, saccule, and semicircular ducts are held in po sition by numerous fibrous bands, identical to the arachnoid membrane, which stretch from the bony walls across the perilymphatic space. The cochlea consists of 1 endolymphatic lumen (cochlear duct) and 2 perilymphatic lumina: the scala vestibuli, which transmits the acoustic fluid wave from the vestibule, and the scala tympani, which allows the fluid wave to decompress at the round window membrane The cochlear duct (scala media) consists of a spirally arranged tube enclosed in the bony canal of the cochlea and lying along its outer wall. The osseous spiral lamina extends only part of the distance between the modiolus and the outer wall of the cochlea; the basilar membrane extends from its free edge to the outer wall, completing the partition that separates the scala media ventrally from the scala tympani dorsally. A more delicate Reissner membrane extends from the thickened periosteum covering the osseous spiral lamina to the outer wall of the cochlea, where it attaches a short distance above the outer edge of the basilar membrane. The Reissner mem-

brane separates the scala vestibuli ventrally from the scala media dorsally. Contained within the cochlear duct (scala media) is the spiral organ of Corti, the auditory apparatus composed of the sensory hair cells, innervated by branches of the cochlear nerve.

1.2 The blood flow of inner ear

The inner ear artery (labyrinthine artery), which is usually a branch of the AICA (Anterior Inferior Cerebellar Artery), nourishes the inner ear, which is composed of the cochlea and the vestibular apparatus. The arterial blood supply to the cochlea is maintained by an artery running spirally within the modiolus, which is the direct continuation of the inner ear artery, and from its terminal branch. There is no functional anastomosis of blood flow disturbance in patients with auditory of blood vessels between the middle ear and the inner ear, in spite of their close anatomical relationship (Figure 2) [2].

Vascular anatomy of mammalian cochlea has been studied in guinea pigs, rats, cats, gerbils, chinchillas, rabbits, mice, monkeys and humans.

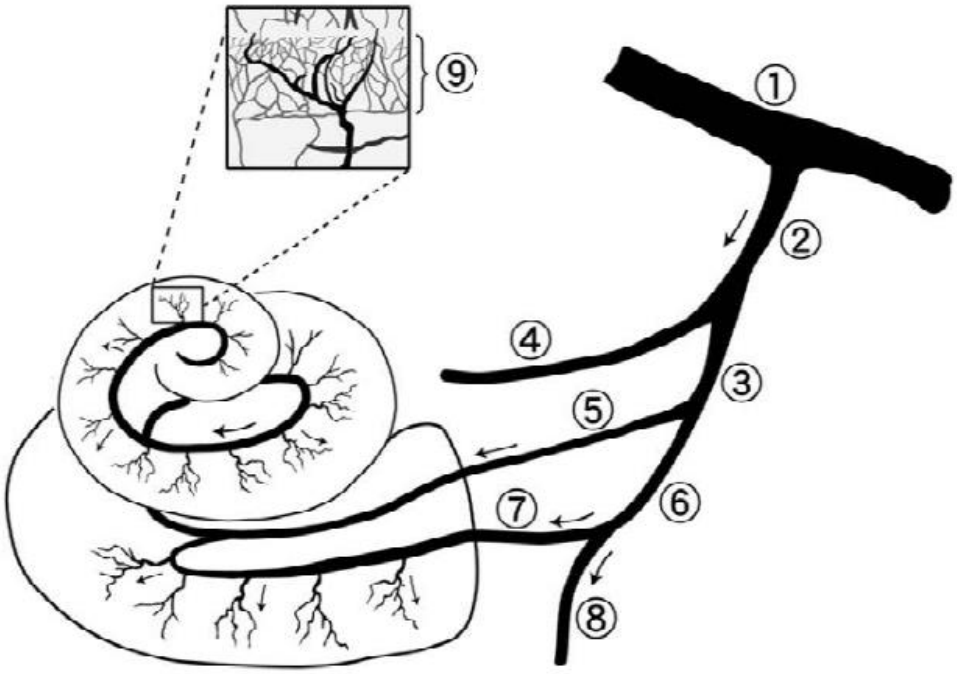

1 – Anterior inferior cerebellar artery (AICA); 2 – Labyrinthine artery (Inner ear Artery); 3 – Common cochlear artery; 4 – Anterior vestibular artery; 5 – Cochlear artery (Spiral modiolar artery); 6 – Vestibulo-cochlear artery; 7 – Cochlear branch and 8 – Vestibular branch; 9 – capillaries of the stria vascularies. Arrows indicate the blood flow directions.

Figure 2 – Schematic view of major arteries from the labyriinthine artery

Arterioles leave the artery running centrifugally and radiate both over the scala vestibuli and across the spiral lamina. The capillary system in the external wall and in the spiral lamina are drained centripetally by radiating collecting venules. In the lateral wall of the cochlea, blood flows from the scala vestibuli towards the scala tympani, and through capillary networks in the stria vascularis at the scala media. The capillaries of the stria vascularis appear to be composed of endothelial cells without smooth muscle cells. The spiral ligament, which is located at the outer layer of the stria vascularis, contains blood vessels morphologically similar to arteriovenous anastomoses. Arterioles coming out from the spiral modiolar artery and running across the spiral lamina. The blood vessels supplying the spiral lamina are similar in appearance to those of the spiral ligament. However, adrenergic fibers were found in the vicinity of blood vessels in the spiral lamina, not in the spiral ligament. In the lateral wall, perivascular adrenergic innervation extends beyond the immediate branches of the modiolar artery and reaches into the radiating arterioles, but not into the area of the scala media. The terminal vessels of the arterioles of the spiral lamina are the vessel of the basilar membrane (VSBM) or the vessel of the tympanic lip (VSTL). The VSBM is located beneath the tunnel of Corti and the VSTL is located close to the VSBM [2].

These two capillary vessels are spiral and parallel. Regarding the VSBM beneath the organ of Corti, there are relatively large inter-species differences. In contrast, the blood vessels in the lateral wall have very similar distribution among species. In humans, the VSBM is relatively continuous.

A great similarity has been observed in the vascular anatomy among mammalian cochleas, and the vascular anatomy of the human cochlea has been described. The venous system of the human cochlea is relatively more complex than other mammals. There are separate venous systems running spirally within the modiolus in close proximity to the scala tympani and the scala vestibuli. The cochlear venous system is also more complicated than the arterial system. The labyrinthine artery supplies the cochlea, whereas the venous system is divided into three vessels; the vein of the cochlear aqueduct (VCAQ), the vein of the vestibular aqueduct and the vein passing through the inner acoustic meatus.

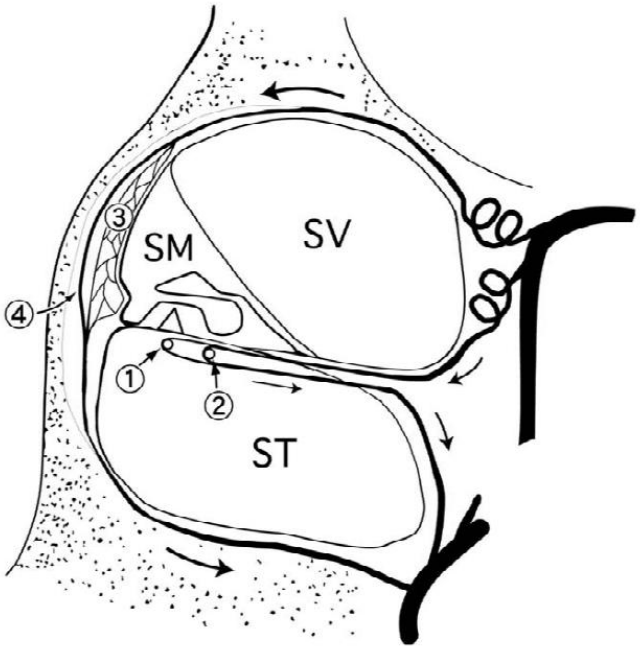

1 – Vessel of the basilar membrane (VSMB); 2 – Vessel of the tympanic lip (VSTL). These vessels are belonging to the spiral portion; 3 – Capillaries of the stria vascularis; 4 – Vessels of the spiral ligament. These vessels are belonging to the lateral portion. Arrows indicate the blood flow direction.

Figure 3 – Schematic view of blood vessels in one cochlear turn. SV, scala vestibuli; SM, scala media; ST, scala tempani

1.3 Volume and distribution of cochlear blood flow

The absolute and relative distribution of cochlear blood flow has been investigated using microspheres in various animals. Cochlear blood flow volume was 1.460.9 ml/ min , 1.8060.8 ml/ min in guinea pigs, 1.6460.49 ml/ min, 1.6460.70 mg/ min in rats, 3.1061.19 mg/ min in cats, 2.3460.71 mg/ min , 2.4860.56 ml/ min, 3.861.1 ml/ min in rabbits, 1.2 ml/ min in gerbils, 2.5861.2 mg/ min in chinchillas, and 0.75 ml/ min in chickens.

In rodents such as guinea pigs or rats, cochlear blood flow was on the order of 1 / 10 000 of total cardiac output, and in rabbits it was on the order of 1 / 100 000 of total cardiac output. In humans, it is estimated that cochlear blood flow is on the order of 1 / 1 000 000 of total cardiac output. Thus, the volume of cochlear blood flow is extremely small compared to the total cardiac output. However, its volume is about four times larger than that in the vestibular apparatus .

And there are no blood flow information about human blood flow of human inner ear. Cochlear vascular areas can be divided into three parts: lateral, spiral and central portions.

The stria vascularis and the spiral ligament are included in the lateral portion and the osseous spiral lamina and the organ of Corti are included in the spiral portion. The modiolus. which contains the cochlear nerve, is the central portion. The arterial blood supply to the cochlea is maintained through the central portion. Because terminal blood vessels in the spiral portion (VSBM and VSTL) have no com-municating blood vessels with the lateral portion except in the developing period of the cochlea, the lateral and spiral portions are clearly divided. The central portion is so designated because part of the arterial blood that enters into the central portion returns without going to the lateral or spiral portion [2].

In animal studies regarding blood flow distribution, the percentage of microspheres is the largest in the lateral portion. In rabbits, more than 80% of microspheres were found in the lateral portion, 9% in the spiral portion and 9% in the central portion

It was measured measured inner ear and brainstem blood circulation while systemic blood pressure was modulated by norepinephrine infusion or exsanguination in guinea pigs. They stated that autoregulation was signifi- cantly stronger in the brain than in the cochlea. Kawakami et al. also stated that cochlear blood flow was autoregulated, but this autoregulation was less than brain blood flow in guinea pigs.

Some studies in the guinea pig, however, have shown flow was reduced to various degrees but recovery was strong intrinsic autoregulation in the cochlea. It was investigated the effect of increased cerebrospinal fluid pressure on cochlear and cerebral blood flow in guinea pigs where cerebrospinal fluid pressure was trans-mitted directly to the inner ear through the patent cochlear aqueduct. They reported that cochlear blood flow was not decreased by the fluid pressure elevation as much as was cerebral blood flow. These differences in results regarding the strength of autoregulation in comparison to cochlear and cerebral blood flow may depend on the differences between the experimental conditions.

Autoregulation of cochlear blood flow was obviously stronger than that of middle ear blood flow in the external carotid artery system [2].

1.4 Non-invaisive methods of innear ear investigations

The temporal bone and especially the inner ear has a highly complex anatomical structure, in which the sensory organs of the cochlea and the vestibular system are contained within a small space together with the sound-conducting system of the middle ear. There are a great many clinical aims for which the highest-possible spatial resolution is required. These include the detection of malformations of the inner ear, anomalies of the arterial and venous structures, the confirmation of

dehiscence of the semicircular canals, the presence and location of inner ear otholits and finally, the verification of endolymphatic hydrops in cases of Ménière's disease [2, 4, 5, 3, 13, 32].

Definition of the fine osseous anatomy of the inner ear can be achieved thanks to the capabilities of modern computed tomography (CT) scanners. Analysis of the soft-tissue constituents of the labyrinth, however, is beyond the scope of X-ray techniques. Both in the present and in the near future, anatomical definition of the membranous labyrinth can be expected from magnetic resonance imaging (MRI). Currently, anatomical definition of the membranous labyrinth in the clinical setting remains a challenge despite significant technological advances. When imaging the labyrinth, it is best to take advantage of the signal-to-noise ratio and spatial resolution provided by 3-tesla scanners. Due to it's fluid contents, the labyrinth is best imaged using T2-weighted scanning protocols. The outlines of the fluid-filled labyrinth are, as a first approximation, identical to the inner surface of its osseous counterpart. It is difficult, to perceive the membranes that separate the endolymphatic from the perilymphatic space [1, 2, 4, 5, 9, 13, 14].

The utricular macula is a horizontally oriented, T2 hypointense 'paddle' outlined by the hyperintense copious perilymphatic fluid and the embedded endolymphatic spaces of the utricle above and the saccule below. The saccular macula is oriented roughly in the sagittal plane and is harder to detect, as only its shallow lateral surface is in contact with the hyperintense saccule with which it contrasts on a T2-weighted image. Whereas the ampullary dilations of the semicircular ducts can easily be shown, the ampullary crests are less perceptible when routine magnetic resonance imaging is employed. The spiral lamina of the cochlea separating the scala tympani from the scala vestibuli is easy to identify using MRI. Attempts to delineate the cochlear duct from the scala vestibuli have been unsuccessful, however, owing to the delicate nature of Reissner's membrane. Likewise, the fine membrane separating the utricle and saccule from their surrounding endolymph is far beyond the scope of clinical imaging. The endolymphatic duct is contained within the osseous vestibular aqueduct. While the latter can be seen routinely on CT images, visualizing the endolymphatic duct/vestibular aqueduct complex is extremely problematic, even where highest-resolution clinical MRI is used. Developing high-resolution MRI to the extreme is not the only option for visualizing the different fluid compartments of the inner ear. A different approach would be to utilize or create different imaging characteristics of endolymphatic and perilymphatic fluid, and to increase their contrast [4, 5, 14, 15].

1.5 Disease associated with the Inner ear malformations

1.5.1 Sensorineural hearing loss

Sudden sensorineural hearing loss (SSNHL) can be defined as an idiopathic hearing loss of sensorineural origin, greater than 30 decibel (dB) in 3 contiguous frequencies that within 3 days. In adults the prevalence ranges between 5 and 20 for 100,000 person/year. It cannot be possible to find out a specific etiologic factor for each patient, in only 10% to 15% of patients, the etiology may be identified. In most patients SSNHL is unilateral. The causes of SSNHL include impaired perfusion of the cochlear artery, viral infection, autoimmunologic response, acute illnesses such as acute external auditory cancers or otitis media, or the presence of earwax can be detected by microscopic ear examinations. From a differential diagnostic point of view, cerebellar artery should be highlighted anterior inferior (AICA) infarction. Moreover, SNHL can be triggered through sudden perilymphatic leakage in the area around the round or oval window. Even though repeatedly discussed in literature, no precise description of any specific location for perilymphatic leakage exists. Fissula ante fenestram (FAF), as first described in 1890 by Siebenmann, is a slit-like space within the bony otic capsule, anterior to the oval window, representing an anatomical variation within the bony labyrinth. Numerous publications in the late 19th and early 20th centuries have already dealt with its structure and anatomical appearance. If present, an FAF can represent a logical weak point for a fistula with possible perilymphatic leakage [2, 10, 14, 23, 24, 25].

In most cases, studies on sudden sensorineural hearing loss (SSNHL) do not distinguish the results between affected ears (single side or a mix of both sides) within samples from homogenous populations. In cases where the side-related effect is addressed, the authors compared the findings from heterogeneous ages populations or only specified to the adults. Although the latter study showed that bilateral SSNHL was likely to occur in older age, with poorer prognosis and pre-existing accompanying diseases, for instance, diabetes or abnormal lipid panel, recent evidences suggests that age may be an important pathomechanism causal for the diversity of SSNHL and it remains unclear whether there is a side-related difference in the clinical features [24]. If viruses or bacteria in the epipharyngeal region exist, serological tests do not confirm that infections damage inner ear; consequently, it does not mean that they are the cause. CMV, rubella, mumps viruses are the most common viral agents that can cause SSNHL. Mumps virus was the most frequent cause of acute unilateral hearing loss, in the near past. The mumps vaccine has prevented the mumps infections and this has leaded to the decreased occurrence of hearing loss caused by mumps virus.

It is assumed in these cases vascular, infectious or autoimmune origin likely. In addition, they may have neurological background diseases (such as stroke), trauma, tumor lesions (vestibular schwannoma) or rupture of membranes of the inner ear [10, 23, 24, 25].

The diagnosis is radiological. It causes bilateral and progressive hearing loss.

1.5.2 Benign paroxysmal positional vertigo

Benign paroxysmal positional vertigo (BPPV) is by far the most common cause of peripheral vestibular vertigo, with a reported incidence of 8% and a lifetime prevalence of 2.4% in a population. BPPV can theoretically affect either of the 3 semicircular canals, but the posterior semicircular canal (pSCC) BPPV is by far the most prevalent. A wide spectrum of symptom severity exists, ranging from mild dizziness to vertiginous episodes, severe enough to cause nausea and vomiting, and significantly impair daily functioning. The classic symptom of pSCC BPPV is episodic vertigo which is invariably precipitated by certain changes in head position relative to gravity; lasts is geotropic and torsional; has brief latency and limited duration; fatigues after repeated testing and reverses upon sitting. The diagnosis of pSCC BPV is based primarily on these classic history and symptoms along with the characteristic clinical signs.

Most cases of BPPV are thought to be idiopatic. It is degeneration of the end organ giving rise to free-floating endolymph debris. In the cupulolithiasis model, deposits become adherent to and load the cupula, rendering it more responsive to gravity. The alternative hypothesis implicates free-floating particles within the canal lumen (canalolithiasis). In this model, gravity pulls the free-floating particles through the endolymph. Due to the viscosity of the endolymph and the hydrodynamic drag, the moving particles create an endolymph current and in turn, cupular displacement. While clinicopathologic studies have indicated that both mechanisms can occur, canalolithiasis appears to be the predominant subtype in typical BPPV. It was shown that the free-floating otoconia within the canal lumen with and without linking filaments, and attached to what appears to be a gel matrix. Otoconia of saccular origin are unlikely to be involved due to its remote location relative to the semicircular canals of the inner ear. Age-related degeneration of the gel matrix and associated linking fibrils, or of the otoconia themselves, may create an environment that is conducive to otoconial detachment and thus the development of idiopathic BPPV. Calcium homeostasis plays a principal role in otoconia formation and absorption. It appears that a similarity exists in the pathophysiology of BPPV and osteoporosis that may highlight calcium metabolism as an etiological factor in BPPV. BPPV can result from inner ear diseases that lead to the deterioration and uncoupling

of otoconia such as sudden sensorineural hearing loss, Meniere's disease or vestibular neuritis [3, 12, 32].

1.5.3 Ménière's disease and endolymphatic hydrops

Meniere's disease is an inner ear disorder characterized by vertigo attacks, fluctuating and progressive hearing loss, tinnitus, and aural fullness in the affected ear. Theories so far are anatomical variation in the size or position of the endolymphatic sac and duct, viral inflammation or autoimmune involvement of the sac, or a genetically determined abnormality of endolymph control. The pathophysiology of Meniere's disease remains unproven and controversial. Based on temporal bone histology (and now magnetic resonance imaging of the inner ear), the fundamental pathophysiological feature of Meniere's disease is endolymphatic hydrops. Postulated causes include anatomical variation and size of the endolymphatic sac and duct, viral infection or autoimmune involvement of the sac, or a genetically determined abnormality of endolymph control [7, 8, 13, 20, 21, 22].

On the basis of cytologic characteristics and functional studies from animal experiments, it has been suggested that the ES (Endolymphatic sac) plays an important role mainly in regulating ion homeostasis and endolymphatic fluid volume. In addition, it is thought to be involved in the immune reaction and in eliminating various inner ear cellular debris and floating otoconia. If there are any pathologic changes to the ES, various inner ear disorders may develop [7, 10, 22].

The ES is situated from the vestibular aqueduct to the posterior fossa dura and consists of a sinus portion, an isthmus portion, an intraosseous portion (rugose portion), and the ES proper (smooth portion) from the proximal to the distal location. The sinus portion is connected to the saccule and utricle via the saccular and utricular ducts, from which the isthmus portion comprises the endolymphatic duct, and the distal portion after the isthmus portion comprises the ES. The isthmus portion and intraosseous portion are situated in the bony canal, called the vestibular aqueduct. The intraosseous portion and the ES proper are subdivided into proximal, intermediate, and distal portions from proximal to distal location. In 1932, Fraser described distended endolymphatic space of the inner ear in a patient with endolymphatic duct obstruction due to otic syphilis. Those findings suggested that the ES is involved in the regulation of endolymph volume. The resorptive function of the human ES is also supported by several cadaveric studies. Tissue around the ES contains loose connective tissue, capillaries, and villi, which are likely to be involved in the development of endolymphatic hydrops in the presence of vasoconstriction and temporary focal ischemia. Recently, periductal channels around the endolymphatic duct, suggested to be involved in fluid absorption in the area of the endolymphatic duct, were observed. The investigators suggested that most fluid absorption in the ES occurs in the proximal portion of the ES, containing the endolymphatic duct, and obstruction of this portion can induce endolymphatic hydrops. As suggested by those studies, early

studies using human ES from patients with Meniere's disease revealed reduced vascularization and increased perisaccular fibrosis. Other findings in the ES of patients with Meniere's disease were attenuated epithelium, collapsed lumen, increased homogenous substance in the lumen of the ES, reduced surface area of the ES, reduced size of the vestibular aqueducts, reduction of the number of luminal folds, and reduction in the number of small canaliculi in ES luminal area. Endolymphatic hydrops is not always related to pathology of the ES, and decompression itself can be effective for the treatment of Meniere's disease. A placebo effect of ES surgery may be another explanation for the relief. The suggested findings generally focused on the explanation of dysfunction of the ES in the regulation of inner ear fluid volume without direct evidence. Although studies of histopathologic changes to the ES in patients with Meniere's disease have been performed for decades, the findings were heterogeneous, and no consensus regarding ES pathology was established, because of the limited number of samples, which were mostly confined to the late stage of Meniere's disease, different diagnostic criteria for enrolled patients, and limitation of objective measurement and analytic methods in the early studies [7, 22].

New studies documenting the age of onset of Meniere's disease show a pattern similar to benign paroxysmal positional vertigo, raising the possibility that the fundamental cause of Meniere's disease might be detached saccular otoconia [8].

1.5.4 Presbycusis

Age-related hearing loss (ARHL) is used synonymously with presbycusis and can be defined as a progressive, bilateral, and symmetrical sensorineural hearing loss due to degeneration of inner ear structures, which affects particularly the high frequencies and begins around the fifth decade of life. Sixteen percent of population in the second decade of life, 50% in the third decade, and almost all patients in the fourth decade show a fall in their hearing threshold in frequencies above 8 kHz, though conventional hearing tests do not detect hearing loss [21].

In 1993, Schuknecht and Gacek classified degenerative changes depending on the location of impairment. He correlated the histopathological changes in the cochlea with hearing tests. Based on this, he divided the ARHL into the following 4 basic types: sensory presbycusis, neural presbycusis, metabolic presbycusis, and mechanical presbycusis. The sensory presbycusis is characterized by degeneration of the organ of Corti, which often results in a primal loss of outer hair cells and in the further course of inner hair cells. Cell loss begins in the basal portion and progresses slowly towards the apex, and therefore the tone audiogram typically reveals elevated hearing thresholds in high frequencies [21].

As we see, many diseases may occur in case of impaired inner ear. This way, it's important to assess this structure to predict mentioned conditions.

2 Magnetic resonance imaging

2.1 Physical principle

The basic physical concepts in MR imaging, the commonly measured quantitative MR imaging tissue parameters (T1, T2, T2*, and proton density [16, 17].

Qualitative and quantitative magnetic resonance (MR) imaging represent separate yet complementary medical imaging techniques. Whereas qualitative MR imaging relies on visual interpretation of tissue contrast resulting from experimental pulse sequence parameters, such as echo time (TE) and repetition time (TR), quantitative MR imaging is based on measurement and interpretation of tissue-specific parameters.

To generate images with contrast between tissue types, MR imaging exploits the effect of magnetic field gradients and radiofrequency (RF) pulses on groups of nuclei within tissues. Nuclei that serve as candidates for MR imaging include those with either an odd number of protons or an odd number of neutrons. Multiple naturally occurring nuclei are available for use in MR imaging, including hydrogen 1 (1 H), oxygen 17, oxygen 16, fluorine 19, sodium 23, and phosphorus 31. Primarily due to its abundance in tissues and high gyromagnetic ratio, hydrogen has become the basis for clinical MR imaging. Commonly represented as a "tiny magnet," hydrogen is depicted as a spinning top with positive charge distributed over the surface of the proton (Figure 4). The movement of this net charge within a closed loop generates a magnetic dipole moment μ oriented orthogonal to the plane of the moving charge. The dipole moment acts in a similar manner to a household magnet. The individual dipoles of hydrogen protons are too small to detect. Instead, when considering the effect of static magnetic fields B0 and RF pulses B1 on magnetic dipoles, it is more useful to consider the effect on the vector sum of a population of dipoles, called the net magnetic dipole M. In the case of a population of hydrogen atoms without an applied net magnetic field, the individual dipoles will be randomly oriented in space, resulting in zero net dipole moment (Figure 5). However, when an external magnetic field B0 is present, a small number of the dipoles will preferentially align with B0 to produce a nonzero net magnetic dipole, which can subsequently be measured (Figure 6). Although M will align with B0, the individual hydrogen proton dipoles incompletely align and continue precessing around the axis of B0, which is commonly used to define the z-axis. The frequency f with which these dipoles precess in a magnetic field is determined by the Larmor equation (Equation 1):

$$f = \frac{\gamma}{2\pi} \cdot B_0 \,, \tag{1}$$

which states that the frequency of precession in a magnetic field is proportional to the applied magnetic field by a predetermined experimentally derived constant, called the gyromagnetic ratio (g), a characteristic of the particular nucleus being used for imaging. In the case of hydrogen, $g/2\pi$ is equal to 42.58 MHz-$^{T-1}$. When an RF pulse B_1 is applied to magnetized tissue at a frequency matching the Larmor frequency, the constituent individual magnetic dipole moments are reoriented in space, resulting in displacement of the net magnetic dipole away from the z-axis by a flip angle α and thus out of alignment with B_0. This produces a net magnetic dipole moment vector that may be separated into components along the z-axis (Mz) and in the xy plane (Mxy), where the latter can be measured (Figure 7).

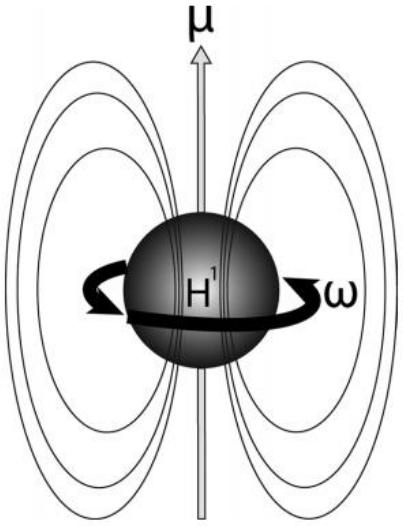

Figure 4 – Hydrogen atom like as a tiny magnet and spinning top

Drawing shows a conceptual hydrogen proton (^{1}H) as a tiny magnet. In this model, the charge of proton is distributed over the surface of the proton and moves in closed loops to produce a magnetic dipole μ, similar to a tiny magnet. The curved arrows represent a precession. Or wooble, of the magnetic dipole about a magnetic field, while ω (radiants/second) represents the angular frequency of this precision. The angular frequency is proportional to the cyclic frequency *f* (cycles/second) by a factor of 2π ($\omega = 2\pi f$) and is determined by the Larmor equation in the presence of a magnetic field. The movement of the charge about the axis of the proton as well as the rotation of the dipole about the axis of an applied magnetic field are analogous to the motion of the spinning top.

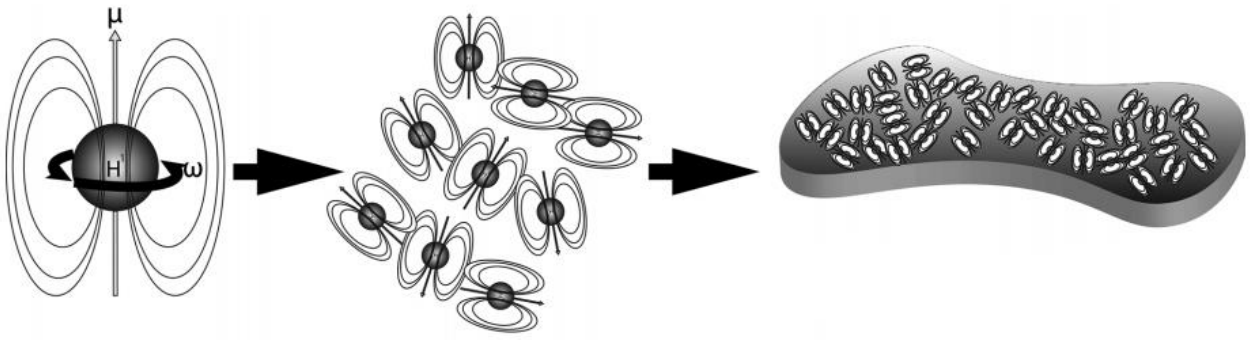

Figure 5 – Populations protons without B_0. Conceptual diagram of the effect of magnetic fields (B_0) is more appropriately applied to large populations of hydrogen protons rather than the individual hydrogen dipole. In this future, where $B_0 = B$, the individual dipoles are randomly distributed in their spin states and orientations, resulting in no net magnetic dipole, $M = 0$.

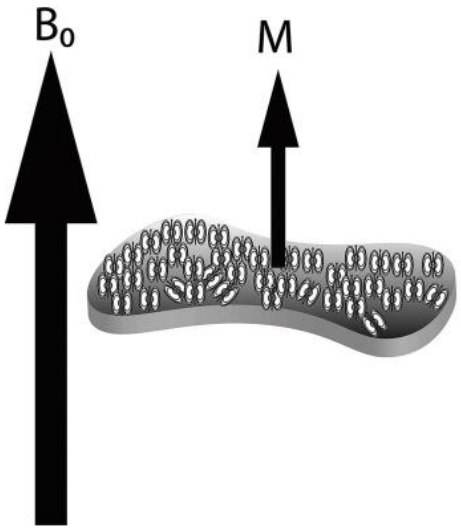

Figure 6 – Non – zero Net Magnetic Field ($B_0 \neq 0$ Tesla). Population of protons with B_0. When a nonzero net magnetic field B_0 is applied, a small number of individual dipoles align with B_0 to produce a nonzero net magnetic dipole *M*

If B1 does not match the resonant frequency of M, then no net change occurs and no measurable signal in the transverse plane is produced. The flip angle a is proportional to the magnitude and duration of the applied RF pulse. Although all individual dipoles contributing to M xy will continue to precess in unison about the z-axis indefinitely under idealized conditions, this is not the case in clinical practice. Because M, and thus Mxy, is produced by multiple smaller groups of magnetic dipoles, differences in the microenvironment alter the speed with which these smaller dipoles precess (Figure 8). Since some precess faster than the others, they appear to spread apart in a process called dephasing. As these dipoles spread, they slowly begin to counteract each other, reducing

the net measurable M xy and producing a free induction decay (FID) curve (Figure 9). While a population of protons exposed to ideal conditions would continue to spin in the xy plane in perfect synchrony following excitation with a B1 pulse to produce a permanent signal, real populations of hydrogen atoms will experience loss of synchrony (dephasing) in the xy plane, causing gradual reduction in the measured xy signal. This is diagrammed with the spreading out of xy-plane vectors. Simultaneously, the z component of magnetism returns with time (red arrow).

Simultaneously, the dipoles begin to realign with B0 to produce an increasing magnetic vector in the z-axis, M z. Although the FID curve generated following an excitation pulse can be measured, steps must be taken to spatially register tissue samples so that meaningful imaging information can be obtained. Application of specialized RF pulses and specialized magnetic fields, termed gradients.

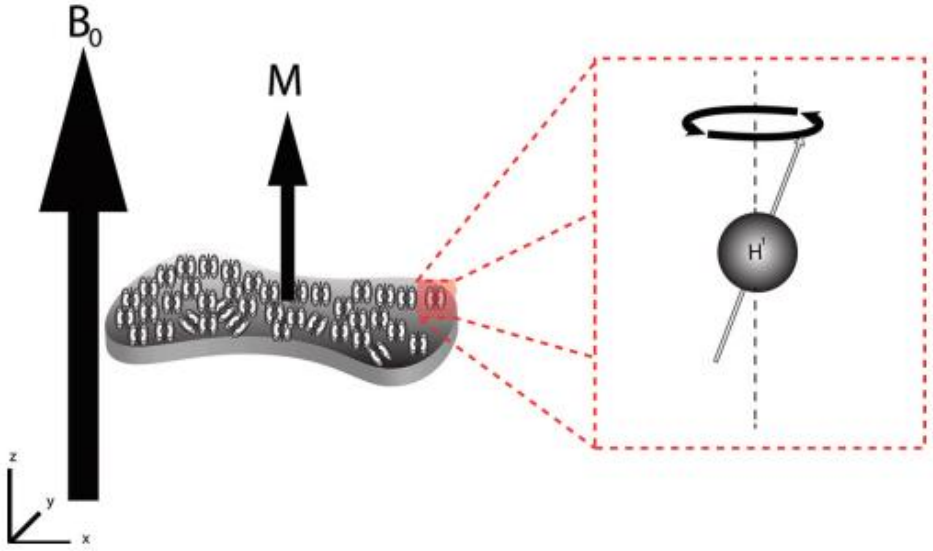

Figure 7 – Continued procession of individual dipoles in B_0. While the net magnetic dipole *M* is aligned with the external magnetic field B_0, the magnetic dipoles of the individual hydrogen protons (shown here without Gaussian lines) continue to precess about the axis of B_0, The frequency of precession is proportional to B_0, based on the Larmor equation

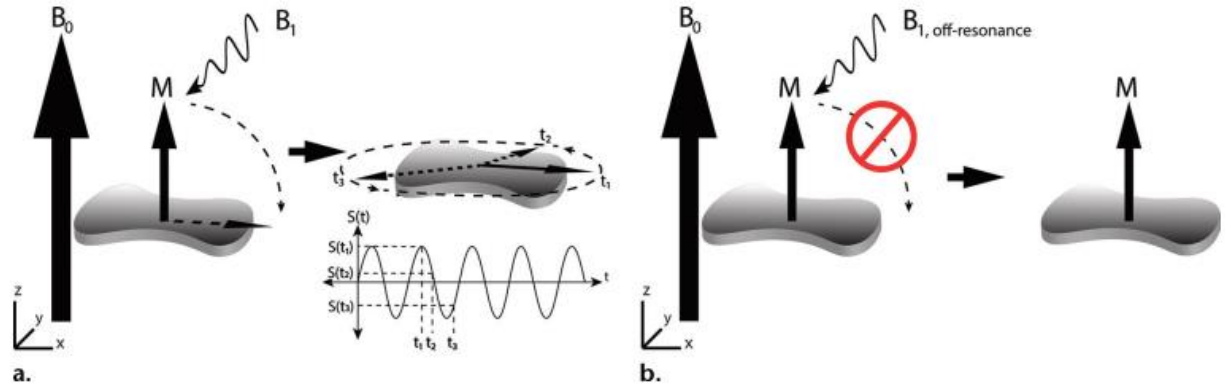

a – When B_1 matches the Larmor frequency, the net magnetic dipole is tipped out of the z- axis by a variable degree to produce a component in the xy plane. The amount of deflection, or flip angle, depends on the duration of the pulse. On discontinuation of B_1, the xy component continues to spin in the xy plane, producing an oscillation magnetic field S (*t*) that may be measured. The graph of S_{xy} (*t*) demonstrates the approximate oscillating appearance of signal as experienced by the receive coil for a very a very short period of time to demonstrate the precession of the net magnetic dipole with time. In true experimental conditions, the signal will decrease with time, as discussed in the text; b – If the frequency does not match, then there will be no deflection of the net magnetic dipole.

Figure 8 – On resonant B_0 and off-resonant B_0

2.1.1 T1, T2 and proton density relaxations

If each group of hydrogen protons discussed earlier responded to RF pulses independent of the local environment, then minimal information of value could be obtained from tissues. The response of hydrogen in tissues is affected by the surrounding macromolecules and elements. The impact of the environment on the detected signal is reflected in T1, T2, T2*, and proton density [16, 17, 26, 27].

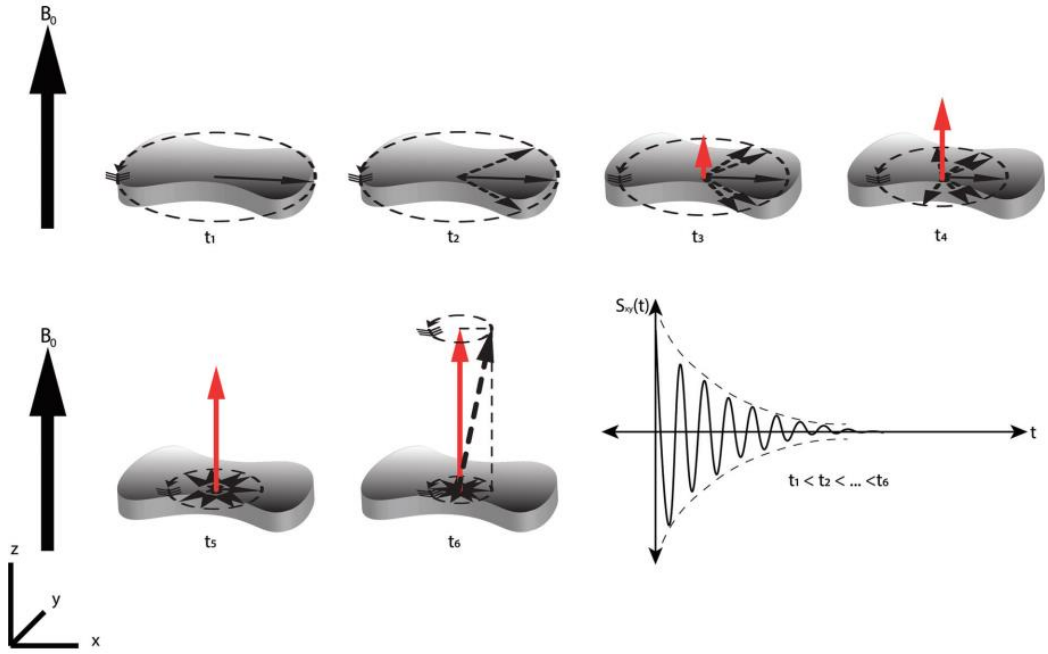

Figure 9 – FID curve. The dashed black arrow shown at time *t*6 represents the net vector produced by both the z-axis and xy-axis components. The signal S(*t*) produced in the xy plane decreases with time, a process called free induction decay.

2.1.2 T1: Spin-lattice relaxation time

The T1 relaxation time, or spin-lattice relaxation time, reflects the exchange of energy between hydrogen protons and the surrounding environment ("lattice"). The lattice acts as an energy reservoir for transfer of energy absorbed during excitation RF pulses. T1 reflects the energy exchange efficiency of the surrounding tissue grid, describing the amount of time it takes for the longitudinal component to return to the equilibrium percentage. This is achieved by local magnetic fields resonating at the Larmor frequency of protons, which cause transitions from high-energy states to low-energy states. T1 reflects the efficiency of energy exchange of the surrounding tissue lattice by describing the amount of time required for the longitudinal component of M, M_z , to return to a percentage of equilibrium. This is accomplished by local magnetic fields resonating at the Larmor frequency of the protons, which induce transitions from high-energy states to low-energy states.

Basic characteristics of T1:

1. TR: short
2. TE: short

On a T1-weighted image, tissues with short T1 look bright. Pulse sequences used to produce T1-weighted images minimize the contribution of the T2 parameter. This is usually achieved by us-

ing a short TR repetition time (300-600 ms) to maximize the difference in longitudinal relaxation during the return to equilibrium, and a short TE Echo Time (10-15 ms) to minimize the contribution of the T2 parameter while receiving a signal.

Tissues and their view on T1-weighted images. Bone marrow: dark; Muscles: gray; Blood: dark; White matter: light; Gray matter: gray; Liquids: dark; Bones: dark; Fat: bright; Air: dark

Pathological processes, as a rule, increase the water content in the tissues. This leads to a loss of signal on T1-weighted images and an increase in the signal on T2-weighted images. Therefore, the pathological processes are usually bright on T2-weighted images and dark on T1-weighted images [11, 16, 17, 26, 27].

2.1.3 T2: spin-spin relaxation time

While T1 represents a tissue property measured with reference to the longitudinal magnetism, T2 or spin-spin relaxation time reflects the amount of time required for the transverse component, M xy , to decrease to a percentage of initial strength in the xy plane following excitation. Since T2 is also influenced by the interaction of spins, which leads to a zero total change in the energy state, the so-called "spin-spin" interactions, T2 is often orders of magnitude shorter than T1. T2 is partially dependent on T1 (spin-lattice) effects, due to progressive loss of phase coherence, when hydrogen interacts with surrounding fluctuating magnetic fields. However, because T2 is also impacted by interactions of spins that result in zero net change in energy state, so-called "spin-spin" interactions, T2 is frequently orders of magnitude shorter than T1. T2*: Reduced Transverse Relaxation Time A derived tissue parameter, the reduced T2 or T2* reflects the combined effect of natural T2 relaxation and relaxation related to static magnetic field inhomogeneities.

These field inhomogeneities can be the result of a nonuniform external field as well as neighboring fields from adjacent tissues, commonly seen at interfaces of tissues, which result in early dephasing of individual magnetic dipoles. Thus, T2* will be shorter than T2 and is determined by the following equation (Equation 2):

$$\frac{1}{T2^*} = \frac{1}{T2} + \frac{1}{T2'}, \tag{2}$$

where 1/T2' is the additional rate of decay in signal caused by magnetic field inhomogeneities.

On a T2-weighted image, tissues with T2 look bright. Pulse sequences used to produce T2-weighted images minimize the contribution of the T1 parameter. This is usually achieved by using a

long TR repetition time (2000-6000ms) to maximize the difference in transverse relaxation during a return to equilibrium, and a long TE Echo Time (100-150ms) to minimize the contribution of the T2 parameter during signal acquisition. Fluid usually looks bright on T2-weighted images.

Tissues and their view on T2-weighted images. Bone marrow: same or lighter than muscle (fat in the bone marrow is usually light); Muscles: gray (darker than muscles in T1-weighted images); Fat: bright (darker than fat on T1-weighted images); White matter: dark gray; Blood: dark; Gray matter: gray; Fluids: bright; Bones: dark; Air: dark

Basic characteristics of T2:

1. TR: long
2. TE: long

Coupling angle: less important than with T1 weighting [16, 17, 26, 27].

Terms such as T1-weighted and T2-weighted understandably often lead to confusion and are often assumed to represent images with pixels reflective of the pure T1 and T2 tissue parameters. Instead, T1-weighted and T2-weighted reflect differences in timing of stages of a pulse sequence. Despite the name, a T1-weighted image actually contains signal related to both the T1 relaxation and T2 relaxation parameters, as well as proton density. A T2-weighted image similarly reflects signal related to these tissue parameters. A simple method to illustrate this point is to inspect the equations modeling the received signal. Consider the equation modeling the conventional spin-echo sequence as applied to a generic tissue sample. In this case, the theoretical signal S obtained in a homogeneous magnetic field will be dependent on the following simplified modeling equation, which has been derived in prior works, to which the reader is referred for an expanded form of the equation (Equation 3):

$$S = S_0\left(1 - \exp\left(-\frac{TR}{T1}\right)\right)\exp\left(-\frac{TE}{T2}\right), \quad (3)$$

where S_0 is the maximal measurable signal, TR is the interval between excitation RF pulses, and TE is the time between the excitation RF pulse and the detected echo. Visual inspection of this equation easily demonstrates how slight alterations in the predetermined TR and TE values can dramatically alter the measured signal (see Figure 10). To weight the study with greater T1 effect, short TR and short TE are selected, whereas for greater T2 effect, long TR and long TE are selected. Despite this weighting, neither T1 nor T2 effects can be completely eliminated. The matter is further complicated clinically by the fact that different classes of pulse sequences weighted to the same parameter will result in images with completely different tissue contrast, as demonstrated in a review of conventional spin-echo and fast spin-echo (FSE) sequences. Comparatively, a map of

quantitative tissue parameters, such as T1 and T2, is independent of pulse sequence parameters. This translates to the fact that images are free of the effect of TE and TR. Pixel values will possess intrinsic value instead of relative value. For example, in contrast to single-section and multisection FSE imaging, where the ratio of cerebrospinal fluid to gray matter can change from 1.6 in conventional spin-echo imaging to 2.4 in FSE imaging, all else being equal, the relative difference in value between the two tissues obtained using a quantitative method will remain constant for a given field strength. To illustrate this concept, consider the effect of varying TR and TE in a pulse sequence called mixed turbo spin-echo (TSE) to produce T2-weighted images (see Figure 11). The qualitative T2-weighted images shown are both acquired at nearly the same time during a mixed TSE sequence. However, owing to differences in experimental effective TE values used for the pulse sequence, the resultant images have different degrees of T2 weighting and consequently different tissue contrast. While the images appear noticeably different, the underlying tissue, and thus the tissue parameters, have not changed between the images. In a PD-weighted image, tissues with a higher concentration or density of protons (hydrogen atoms) look bright. This is usually achieved by minimizing the effects of T1 and T2 differences, using the long TR repetition time (2000-5000ms) and short TE (10-20) (Figure 10, Figure 11).

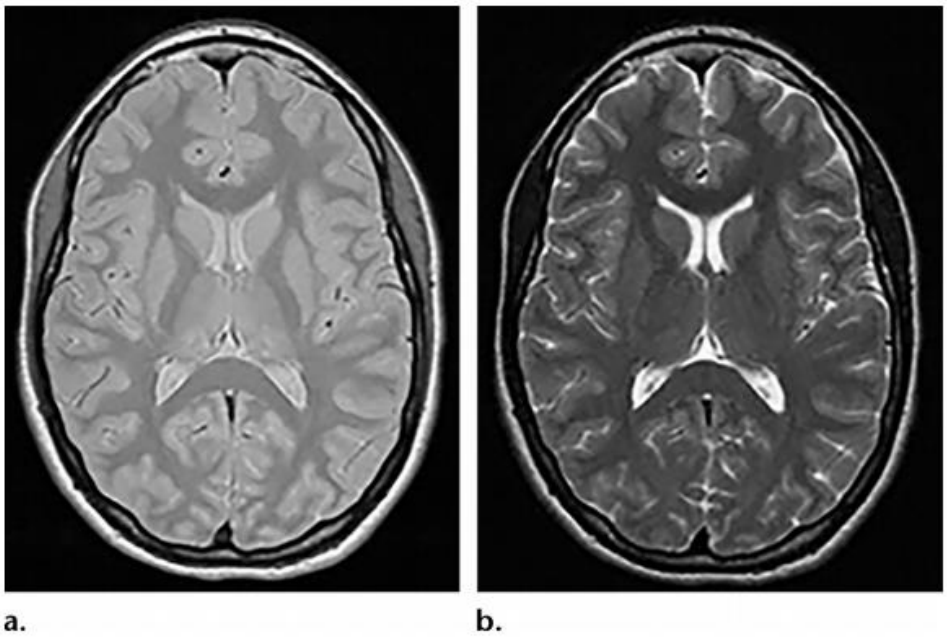

a – T2 Sequence with the Short TE, tissues look bright, b. – T2 Sequence with the Long TE, tissues look dark.

Figure 10 – T2 tissue weighting. Directly acquired T2-weighted images obtained using a mixed TSE quantitative pulse sequence demonstrate how the tissue contrast varies on the basis of the relative T2 weighting, which is controlled by manipulating the TE

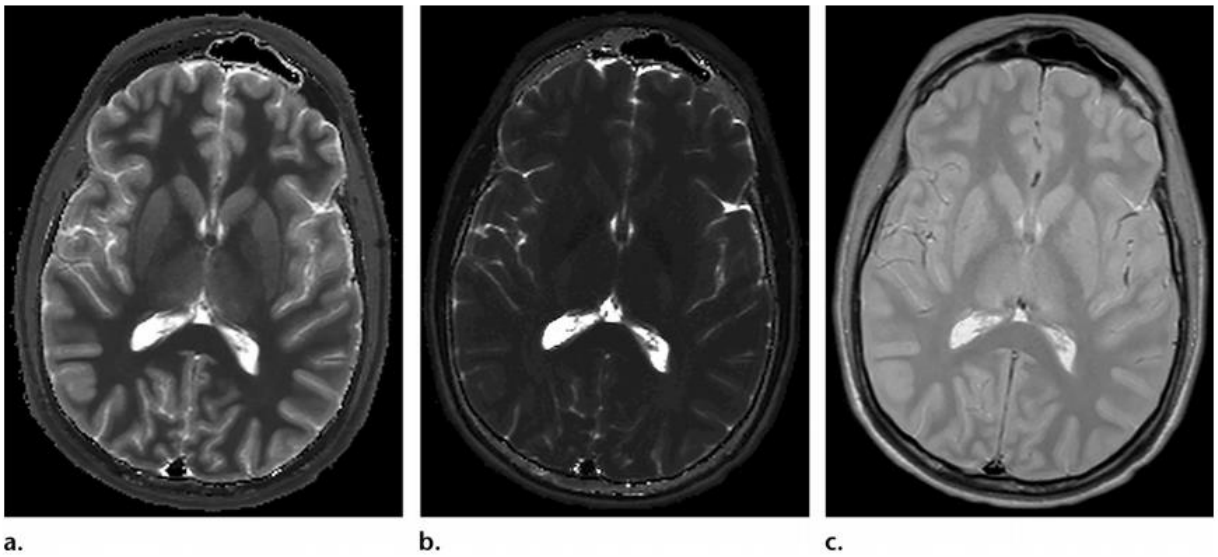

Axial T1 (a), T2 (b), and proton density (c) tissue parameter maps calculated from data acquired using a mixed TSE quantitative pulse sequence at the level of the lateral ventricles. Although tissue parameter maps may demonstrate tissue contrast similar to that of their qualitative counterparts, as is the case with the T2 parameter map (b), the major important concept regarding parameter maps is that the value of each pixel is proportional to the associated tissue parameter.

Figure 11 – Tissue parameter maps

2.1.4 Proton density

Proton density represents a physical parameter, a parameter proportional to the concentration of hydrogen atoms and therefore present in the absence of B_0. For clinical purposes, the measured parameter can be taken to reflect the total number of protons. The facts that proton density is a time-independent variable and is commonly grouped with a number of variables in equations used to calculate tissue parameters distinguish it from the other parameters.

Basic PD characteristics:

1. TR: long
2. TE: short

PD weighted images.

On PD-weighted images with fat saturation, adipose tissue (areas containing adipose tissue, for example, subcutaneous fat and bone marrow fat) look hypo intense [16,17,26,27].

2.2 Quantitative MR imaging technique

Although the concept of quantitative MR imaging is intuitive when broken down into its basic components, the sheer number and sometimes indecipherable complexity of pulse sequences can deter many from investigating quantitative MR imaging as a potential clinical tool. Rote memorization of the components of each pulse sequence is inefficient, exhausting both time and resources. Employing a hierarchical modular approach to pulse sequence design can help reduce the complexity of pulse sequences. This can be accomplished by first understanding that all pulse sequences are based on repeatedly applying RF pulses to a volume of tissue to generate an image and can be divided into the following steps: pre-excitation weighting, excitation, postexcitation weighting, and spatial encoding and readout (Figure 12). Subsequent understanding of pulse sequence hierarchy simply involves grouping pulse sequences on the basis of minor modifications to each of these four stages [16, 17, 26, 27].

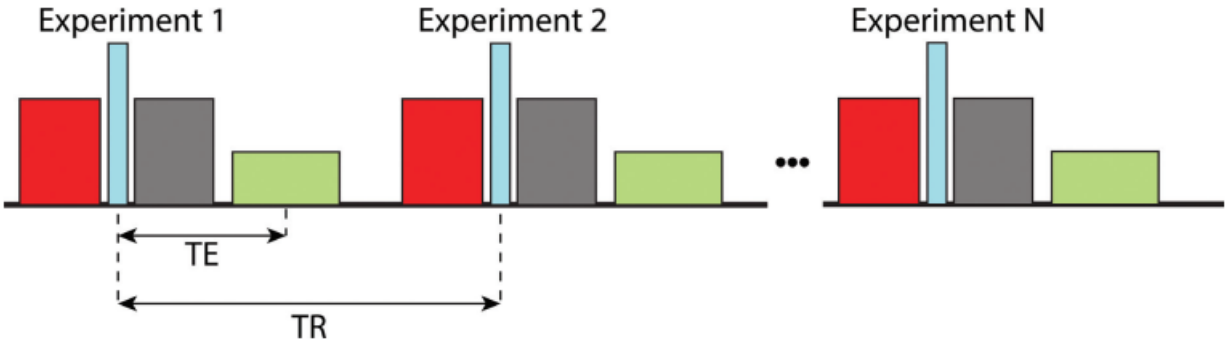

Figure 12 – Conceptual diagram for modular pulse sequence design. While full pulse sequence diagrams may appear complex, all can be reduced to four components. The four steps include pre-excitation weighting (red box), excitation (blue box), postexcitation weighting (gray box), and spatial encoding and signal readout (green box). These steps need to be repeated multiple times to produce an image

2.2.1 Conventional spin-echo

This technique applies a 180º inversion pulse at time τ, or TE/2, to the sample to cause the precessing M xy components to flip in the xy plane, where they continue to precess at different speeds relative to one another, but now in such a way that the individual dipoles realign at time 2τ, or TE. The signal produced is called a spin echo.

By adjusting the TR and TE time variables, we can get T1, PD, and T2 weighted images, while T2 and PD weighted images can be obtained using double or multi-echo sequences. All spin-echo sequences include 90 ° and one or more 180 ° dephasing pulses. After applying a 90 ° excita-

tion pulse, the total magnetization is in the XY plane. Immediately begins the phase shift of the protons due to T2 relaxation time (spin-spin interaction) and the signal abruptly decreases. Shortly after the 90° RF pulse applies a second 180° RF pulse that causes the spins to rephase. When all spins are restored in phase, the signal becomes high again. Conventional spin-echo represents one of two parent sequence designs and uses only postexcitation modifications. Following a 90º sectionselected excitation pulse, a postexcitation module consisting of frequency- and phase-encoding gradients and a single section-selected 180º refocusing pulse is applied at TE/2, resulting in realignment of magnetic dipoles at time TE to produce a single spin echo. The process is repeated after time interval TR, where TR is selected such that TR is much greater than T1 to maximize measured signal (see Figure 13). Multiecho spin-echo sequences follow the same modular design, as will be discussed regarding the QRAP-MASTER sequence (quantification of relaxation times and proton density by multiecho acquisition of a saturation recovery using turbo spin-echo readout). However, they have multiple section-selected refocusing pulses at regular intervals, and while possessing only a single phase-encoding gradient, require the application of multiple frequency-encoding gradients. Data acquired with conventional single-echo spin-echo imaging can be used to solve for tissue parameters using the simplified modeling equation. Conventional spin-echo represents a standard of reference for pulse sequences used for parameter mapping due to its high reliability, with minimal motion artifact and relative insensitivity to magnetic field inhomogeneities. Tissue parameters that may be derived from conventional spin-echo imaging include T1, T2, and proton density. The latter parameter is grouped as part of the term representing the maximal signal S_0.

1. The received signal is called an echo, because it is “recovered” from the FID signal.
2. A 180 ° rephasing pulse follows exactly in the middle between a 90 ° pulse and an echo.

Benefits

1. Strong signal.
2. Compensation of local field inhomogeneities: fewer artifacts.

disadvantages

1. It takes time to complete the rephasing step, which increases the overall scan time.

2. The number of RF acting on the body (not that it is dangerous, but there are certain limitations).

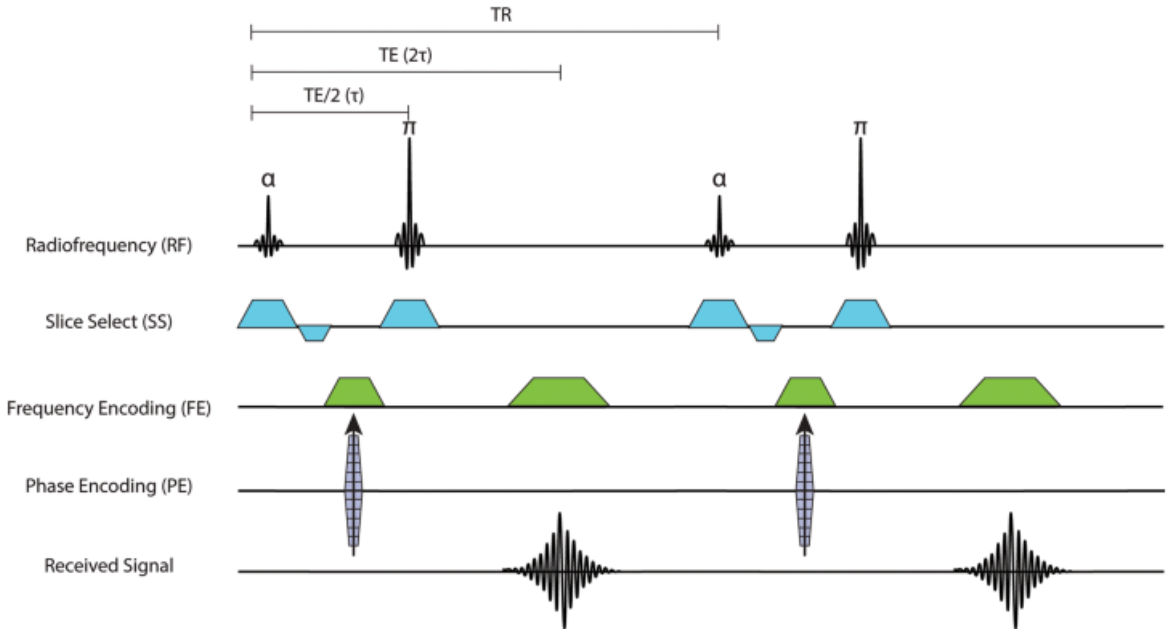

Figure 13 – Conventional spin-echo sequence. Following excitation pulse α, a frequency-encoding gradient is applied. A 180º inversion pulse π is applied at the same section location using a section-select gradient. Subsequently, a phase-encoding gradient is applied to complete spatial encoding. A spin echo resulting from rephasing of the individual dipoles is generated at time TE following the initial excitation pulse α. After a time interval TR, the pulse is repeated.

2.2.2 Conventional gradient-echo

An alternative approach to producing signal is called the "gradient echo," in which the dephasing process is accelerated by applying an additional magnetic field across the transverse plane to change the Larmor frequencies of the individual dipoles in a predictable fashion. The gradient is turned off for a period of time, after which an equal gradient is applied, but in an opposite direction. This allows the individual dipoles to realign. The gradient is unable to reproduce signal as effectively as an inversion pulse, resulting in a smaller signal at any given time.

Gradient-echo represents the second of two parent modular sequence designs, and as with spin-echo, consists of only a postexcitation module to produce signal. Unlike conventional spin-echo imaging, which uses a 90º pulse and a 180º refocusing pulse to produce an echo, conventional gradientecho imaging frequently uses an excitation pulse of less than 90º followed by two sets of frequency gradients to produce an echo. Following the lowangle excitation pulse, the first frequency-encoding gradient is applied with the phase-encoding gradient to cause sequential dephasing of

signal. Subsequently, a gradient of the opposite magnitude is applied to generate a signal at TE by reversing the effects of the first gradient. Unlike the refocusing pulse in conventional spin-echo imaging, the refocusing gradient cannot completely reverse the dephasing effects that occur primarily before a time equal to TE, resulting in a dependence on the reduced T2, T2* (see Figure 14). The signal received by the scanner is modeled by the following simplified equation (Equation 4):

$$S = S_{eq}\left(1 - \exp\left(-\frac{TR}{T1}\right)\right)\exp\left(-\frac{TE}{T2^*}\right), \tag{4}$$

where S_{eq} is the equilibrium signal using full excitation and signal recovery. Early adoption of the gradient-echo sequence for imaging was driven primarily by the speed of imaging. Because low-angle excitation pulses could be used, less time was required to regain sufficient longitudinal magnetization for a subsequent gradient-echo sequence to be applied. A notable difference in the signal obtained from conventional gradient-echo sequences compared with spin-echo imaging is that while the conventional spin-echo refocusing pulse reverses the effects of field inhomogeneities, the frequency gradients in gradient-echo imaging do not, resulting in a dependence on T2*, as shown earlier. Therefore, data acquired for conventional gradient-echo imaging can be used to calculate T1, T2*, and proton density effects [16, 17, 26, 27].

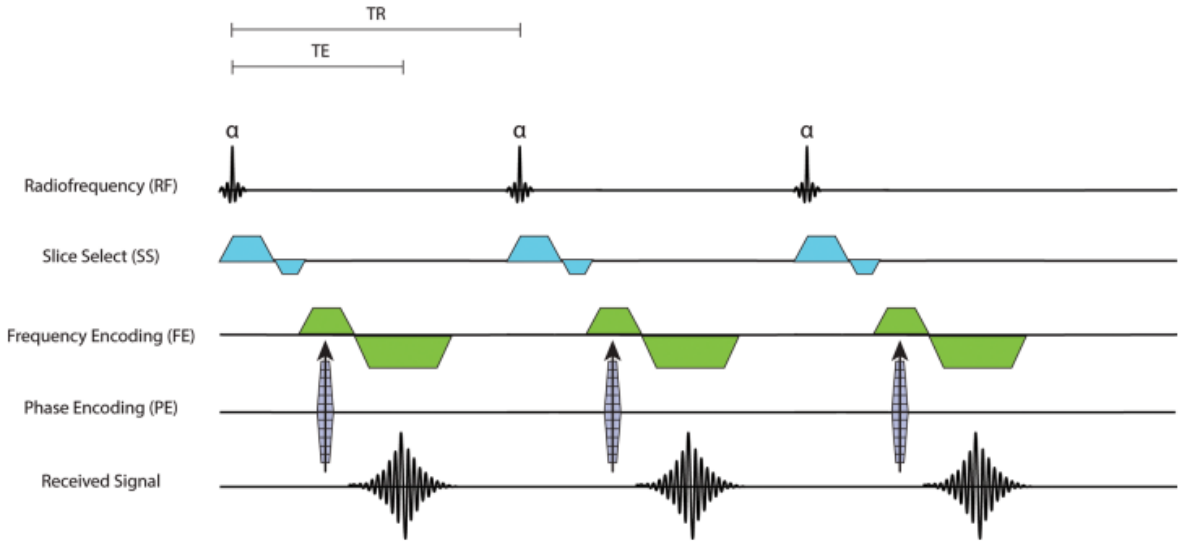

Figure 14 – Conventional gradient-echo imaging. Following excitation pulse α, phase- and frequency-encoding gradients are applied, resulting in dephasing of the xy component. Subsequently, an additional gradient is applied to rephase the transverse magnetization, resulting in a gradient echo at time TE. The sequence is repeated at time TR

2.2.3 TOF (time – of – flight) and DWI

The TOF angiography method is based around a conventional 2D or 3D gradient echo (GRE) sequence with optional gradient-moment nulling. A presaturation pulse is often applied above or below each slice to reduce signal from traversing veins. Moderate-to-large flip angles (30°−60°) are used to maximize contrast between stationary tissue and blood. Short TE values (< 7 msec) are preferred to minimize signal losses from phase dispersion.

Maximal enhancement of flow occurs when the vessel is perpendicular to the plane of imaging. TOF techniques are thus somewhat insensitive to in-plane flow.

The easiest way to identify TOF images, find the blood vessels of the body (Circle of Willis, carotid arteries). On the images of the TOF series, the vessels look bright.

DWI (Diffusion weighted images).

Diffusion imaging is an MRI method that produces in vivo magnetic resonance images of biological tissues sensitized with the local characteristics of molecular diffusion, generally water. MRI can be made sensitive to the motion of molecules. Regular MRI acquisition utilizes the behavior of protons in water to generate contrast between clinically relevant features of a particular subject. The versatile nature of MRI is due to this capability of producing contrast related to the structure of tissues at the microscopic level. In a typical weighted image, water molecules in a sample are excited with the imposition of a strong magnetic field. This causes many of the protons in water molecules to precess simultaneously, producing signals in MRI. In T2-weighted images, contrast is produced by measuring the loss of coherence or synchrony between the water protons. When water is in an environment where it can freely tumble, relaxation tends to take longer. In certain clinical situations, this can generate contrast between an area of pathology and the surrounding healthy tissue.

To sensitize MRI images to diffusion, instead of a homogeneous magnetic field, the homogeneity is varied linearly by a pulsed field gradient. Since precession is proportional to the magnet strength, the protons begin to precess at different rates, resulting in dispersion of the phase and signal loss. Another gradient pulse is applied in the same magnitude but with opposite direction to refocus or rephase the spins. The refocusing will not be perfect for protons that have moved during the time interval between the pulses, and the signal measured by the MRI machine is reduced.

The ratio of the histological structure of the tissue and the diffusion rate are reduced to the fact that the density of the location of cells and a decrease in the volume of extracellular space lead to a decrease in diffusion. Diffusion is especially helpful in the diagnosis of tumors and cerebral ischemia.

The degree of diffusional suspension depends on the area of the diffusion gradient, the interval between the gradients, the effect of spatial localization of the gradients and the size of the voxel:

– stationary water molecule (spin / proton) - is not exposed to diffusion gradients and retains its signal;

– a mobile water molecule (spin / proton) - acquires a phase shift under the influence of the first gradient and does not recover at the next pulse and, therefore, loses the signal [16, 17, 28, 29].

2.2.4 Inversion-recovery

Although commonly taught as a separate entity, the inversion-recovery pulse sequence uses either conventional gradient-echo or spin-echo sequences with the addition of pre-excitation modifications. In the pre-excitation stage of the sequence, an initial 180º inversion pulse is applied. This is followed by a predetermined inversion time (TI) before the excitation pulse. The TI allows T1 relaxation of a selected tissue type such that zero net magnetic vector (and thus signal) will be associated with images produced by the subsequent pulse sequence. Following the TI, an excitation RF pulse is applied and the steps of either the conventional spin-echo sequence or gradient-echo sequence are applied (Equation 5). Alternatively, when the gradient-echo module is used. An inversion-recovery pulse sequence with a conventional spin-echo postexcitation module, recognizing that the gradient-echo module can be substituted (Equation 6 and Figure 15) [16, 17].

$$S = S_{eq}\left(1 - 2 \cdot \exp\left(\frac{TI}{T1}\right) + \exp\left(\frac{TR}{T1}\right)\right)\exp\left(\frac{TE}{T2}\right) \quad (5)$$

Equation 5 for modeling the signal obtained with the inversion-recovery sequence when the spin-echo module is used in the postexcitation portion of the sequence.

$$S = S_{eq}\left(1 - 2 \cdot \exp\left(\frac{TI}{T1}\right) + \exp\left(\frac{TR}{T1}\right)\right)\exp\left(\frac{TE}{T2^{*}}\right) \quad (6)$$

Equation 6 for modeling the signal obtained with the inversion-recovery sequence when the gradient-echo module is used in the postexcitation portion of the sequence.

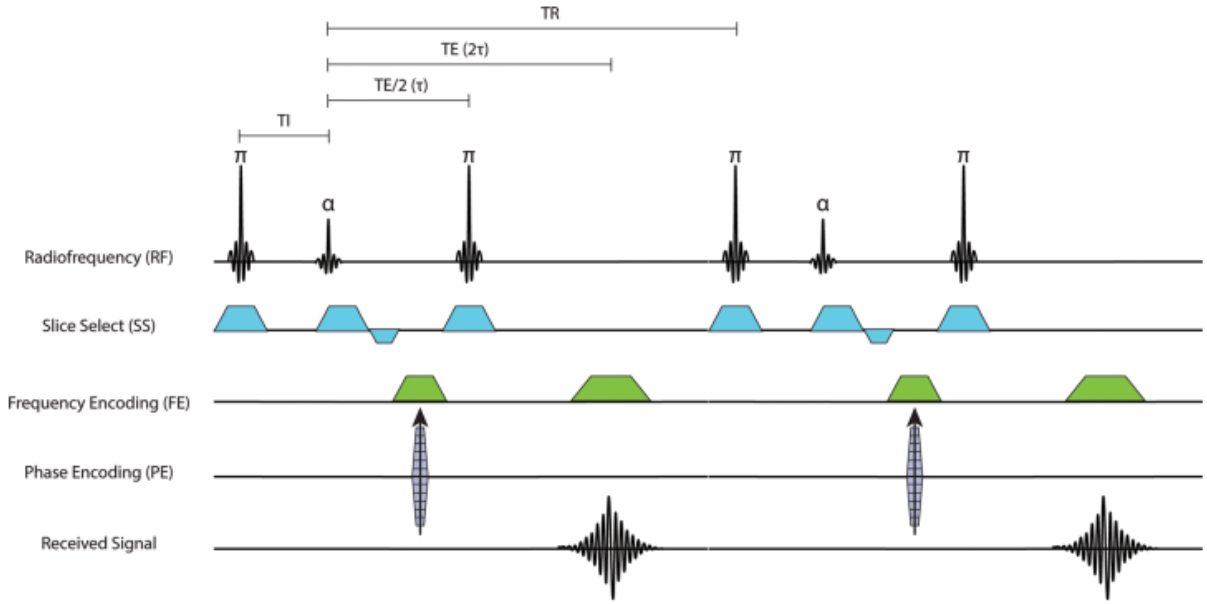

Figure 15 – Inversion-recovery sequence with spin-echo module. The pre-excitation step of a section-selective inversion pulse π is applied. Following a TI delay, either a spin-echo or gradient-echo module may be applied. Here, the spin-echo module is diagrammed

2.2.5 Flair

Flair is one variation of the inversion-recovery sequence. In the flair sequence, the signal from the fluid is quenched by using a long TE and a long TI. An inversion recovery sequence with a long inversion time (TI) of 2000-2500ms is used to suppress fluid. This sequence is usually used in studies where lesions usually overlap with a strong signal from the cerebrospinal fluid. A long TI inversion time suppresses the high level signal from CSF and improves the visualization of small lesions in the periventricular areas and spinal cord lesions [17, 30].

On images produced by the flair method, CSF and other fluids in the brain or spinal cord appear dark, resulting in lesions or other pathological processes that appear bright.

Fabrics and their appearance on flair images; Bone marrow: same or lighter than muscle (fat in the bone marrow is usually light); White matter: dark gray; Blood: dark; Gray matter: gray; Muscles: gray; Fat: bright; Liquid: dark; Bones: dark; Air: dark

2.3 Hybrid pulse sequences

The sequences discussed earlier represent the standard qualitative pulse sequences and serve as the model for subsequent generations of pulse sequences for quantitative MR imaging. Newer hybrid pulse sequences represent modification of conventional spin-echo and gradient-echo imaging

and include FSE or rapid acquisition with relaxation enhancement (RARE), echo-planar imaging (EPI), and gradient- and spin-echo (GRASE). The major benefit of these sequences over the conventional sequences is speed of acquisition of a single tissue parameter [16, 17].

2.3.1 Fast spin-echo and echo-planar imaging

FSE represents an important extension of the conventional SE sequence. After an initial excitation pulse, however, instead of a single refocusing pulse for each TR, multiple 180º refocusing pulses are applied with unique spatialencoding gradients to cause repeated uniquely encoded echoes. Because this pulse sequence does not require a delay for longitudinal relaxation, it can dramatically decrease the persection imaging time by a factor proportional to the number of 180º refocusing pulses applied per TR (echo train length [ETL]) (Figure 16).

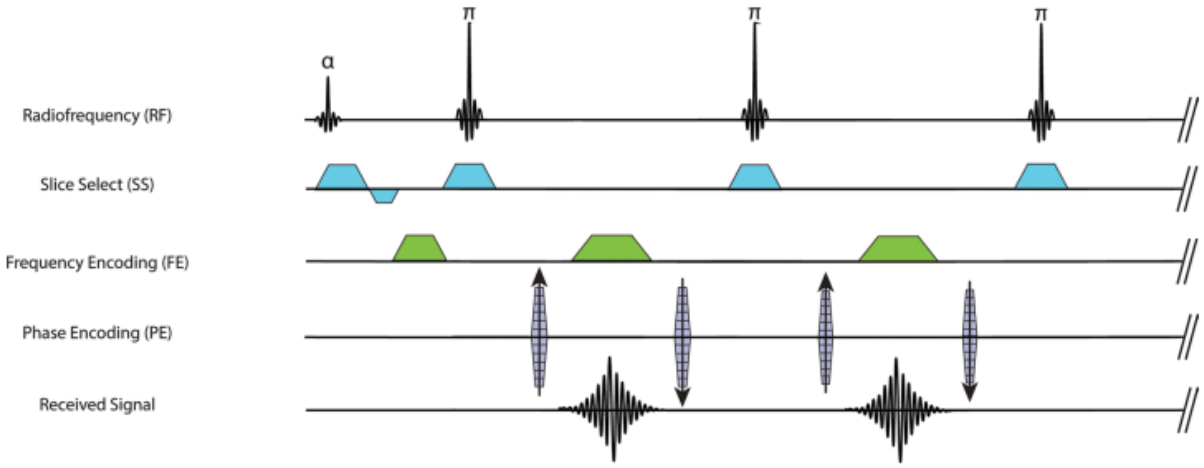

Figure 16 – FSE sequence. Traditional FSE imaging requires no pre-excitation pulse modifications. Following the excitation pulse α, repeated 180º inversion pulses π are applied to generate spin echoes. A key distinguishing feature of FSE imaging is that both phase- and frequency-encoding gradients are applied following each inversion pulse to produce unique spatial data

As expected based on the similarity to conventional spin-echo imaging, FSE signal intensity at the nth echo is a function of T1, T2, and proton density (Equation 7):

$$T_D = \mathrm{TR} - 2N\tau\,, \tag{7}$$

where N is the total number of refocusing pulses for each TR. From its inception, FSE imaging was recognized for its speed over conventional spin-echo imaging. Additionally, FSE imaging confers increased contrast between tissues, assisting in lesion detection. Although the other hybrid pulse

sequences discussed later demonstrate greater speed of acquisition, FSE imaging retains the property of insensitivity to magnetic field inhomogeneities seen in spin-echo imaging. Similar to conventional spin-echo imaging, FSE imaging permits calculation of T1, T2, and proton density; however, as with conventional spin-echo imaging, multiple experiments are required, with each set of data capable of calculating a single tissue parameter (Equation 8).

$$S_n \propto I_n = I_0\left(1 - F\exp\left(-\frac{T_D}{\mathrm{T1}}\right)\right)\exp\left(-\frac{\mathrm{TE}_n}{\mathrm{T2}}\right) \tag{8}$$

Equation 7 for modeling the signal intensity of the FSE sequence at the nth echo.

Echo-Planar Imaging Unlike FSE, which always begins as a spin-echo sequence, EPI pulse sequences can begin as either a spin-echo or gradient-echo sequence. The modular design of conventional spin-echo or gradient-echo sequences is followed by successive rapid fluctuations in frequency-encoding gradients to generate a gradient-echo train with repeated phase-encoding steps.

A modified version of this sequence was created using a pre-excitation inversion pulse followed by multiple EPI pulse sequences. The equation used to solve for tissue parameters using this modified inversion-recovery gradient-echo EPI readout at step pulse readout number n, where 1 < n < m, is defined by Equation:

$$S_n = \int_{-\infty}^{\infty}\left(M_n(z)\cdot\sin\varphi(z)\cdot\exp\left(\frac{\mathrm{TE}}{\mathrm{T2}^*}\right)\right)dz, \tag{9}$$

where TR is much greater than T1, Tb is time between excitation pulses, and the following are true

$$\alpha(z) = \cos(\phi(z)), \tag{10}$$

$$\beta = \exp\left(-\frac{T_b}{\mathrm{T1}}\right), \tag{11}$$

$$\gamma = \exp\left(-\frac{\mathrm{TI}}{\mathrm{T1}}\right). \tag{12}$$

Despite representing one of the oldest pulse sequences, EPI found its way into clinical practice only with advancements in computer processing speeds. It was soon recognized for its speed, capable of imaging a volume of tissue in milliseconds, compared with minutes for conventional spin-echo imaging. The gains in speed are proportional to the echo train length, similar to FSE imaging. Although EPI is faster than FSE imaging, qualitative imaging can be limited by artifact from T2* effects, at times requiring the sequences to be converted from single-shot to multishot acquisition—where the sequence is performed multiple times, rather than once— to obtain a complete data set for the imaged tissue. As with other gradient-echo–based sequences, EPI is dependent on, and may be used to calculate, T1, T2*, and proton density. Gradient- and Spin-Echo Owing to early limitations of EPI, including hardware and spatial resolution, the GRASE pulse

$$F = \left(\frac{1 + (-1)^{N} \exp\left(- \frac{2N\tau}{\mathrm{T1}} 1 \right) \left(\cosh\left(\frac{\tau}{\mathrm{T1}} \right) - 1 \right)}{\cosh\left(\frac{\tau}{\mathrm{T1}} \right)} \right) \qquad (13)$$

sequence was designed to combine the attributes of FSE imaging and EPI. The modular design of the GRASE sequence is a hybrid of EPI and FSE imaging. The first portion consists of typical spin-echo excitation steps and is followed by both frequency- and phase-encoding gradients to produce multiple gradient and spin echoes. A second refocusing pulse is applied and the gradient steps are repeated. Subsequent refocusing pulses with accompanying gradients can be applied until k- space is filled. The modeling equation for the GRASE sequence is similar to that for FSE imaging; however, as would be expected from pulse sequences incorporating gradient echoes, it additionally incorporates the T2* tissue parameter effects. Additionally, GRASE imaging offers the potential for improved signal-tonoise ratio compared with those of FSE imaging and EPI, if all other parameters are held constant. Unfortunately, GRASE imaging is susceptible to similar limitations as experienced by EPI and FSE imaging related to technological limitations, specifically eddy currents, phase errors, and gradient and receive train group delay errors [16, 17].

2.3.2 MPrage

MPRAGE - For imaging, a 180º degree primary pulse inversion is used, followed by a sequence of gradient echo signals that form an image (steady state using rewind gradients). To obtain a 3D image, the secondary phase is encoded in the direction of the selected slice. Only one segment or section of a 3D data recording receives a preliminary pulse. After receiving the signal from all lines within the 3D image, the delay time TD (Time Decay) follows. It is necessary to prevent the appearance of saturation effects. The MPrage series is commonly used for high resolution 3D isotropic imaging of the brain. Compared to the T1-weighted SE sequence, MPRage provides superior image quality and better contrasting gray and white matter.

The T1SE and MPrage series are similar. The only significant difference between the series is the better contrast between the gray and white matter in the MPRAGE images. The MPRAGE series produces high-resolution isotropic 3D images, and after obtaining them, a multi-plane reconstruction is possible.

Tissues and their visualization on MPRAGE images. Bone marrow - looks identical or brighter than muscle (fatty bone marrow is usually bright); Circulating blood - gray (bright after contrast); White matter is saturated white (and looks brighter than on T1SE images); Gray matter gray; Liquids – dark; Muscles – gray; The bone is dark; Fat – bright; The air is dark [16,17,31].

2.4 Perfusion imaging

Perfusion refers to the delivery of oxygen and nutrients to tissue by the blood flow. The evaluation of the microcirculation in MR is based on the use of a "tracer" of the vascular compartment and recording of the distribution of this tracer over time in the organ of interest. The tracer can be exogenous (mainly gadolinium chelates) – DSC. DSE, Presto or endogenous (magnetized water molecules in the in-flowing blood) - ASL.

Dynamic MRI consists of fast repeated acquisitions of the same tissue volume before the administration of a bolus of gadolinium contrast medium and during its pass in the organ of interest over a fixed period of time. Following contrast administration, signal changes are induced by changes in either T1 or T2 relaxation or susceptibility-related effects. The signal changes following the contrast bolus are used to probe the vascular properties of tissues. Four different types of fast sequences can be used: T2*- weighted EPI (dynamic susceptibility contrast (DSC)), PRESTO or T1-weighted 2D/three-dimensional (3D) fast gradient echo (GRE) sequence (dynamic contrast enhancement (DCE)), Arterial spin labelling (ASL).

2.4.1 DCE and DSC

Injection rate and temporal resolution DSC mainly focuses on studying the first pass of the contrast agent (the first minute after the injection of Gd), while DCE investigates the contrast agent uptake and equilibrium in the brain tissue (over a range of 5–15 min). This influences the injection rate, which is high for DSC perfusion (>5 ml/s), in order to achieve a compact and concentrated contrast medium bolus, and lower for DCE (usually about 3 ml/s or less), in order to get an arterial input function that is easier to sample.

The choice of the appropriate DCE-MRI acquisition technique largely depends on factors such as spatial coverage, temporal sampling rate, and magnetic field strength. For DSC-MRI, a free-induction decay EPI (FID-EPI) or a spin-echo (SE-EPI) sequence can be used. The SE exhibits a sensitivity to smaller vessel sizes that corresponds to the diffusion distance of a water molecule during the echo time. The FID-EPI sequence is preferentially used; it has a sensitivity to all vessel diameters and a larger response (SNR increase) to a given contrast agent concentration compared to SE-EPI.

Following data acquisition, signal changes are analyzed with various MRI and pharmacokinetic models, and quantitative microvascular indexes can be derived. The Gd contrast agent (CA) concentration can be estimated either from the MRI signal enhancement (DCE) or decrease (DSC). The Figure 18 shows a visual assessment of the signal variation in glioblastoma for these two types of dynamic acquisitions, as well as two examples of derived quantitative maps. For DSC-MRI, relative cerebral blood volume (rCBV), flow (rCBF), and mean transit time are calculated using simple deconvolution. The increased sensitivity and accuracy of the Bayesian reconstruction at lower SNR allows one to further reduce the contrast agent dose and, since automatically shortening the bolus length, it also improves the quantitative estimation. For DCE-MRI, in addition to dynamic data, predetermined values of T1 or pre-contrast reference data are required to enable the estimation of the initial tissue T1 relaxation time, which then permits the conversion of the DCE-MRI signal intensities into Gd concentrations. Then, given the Gd concentration as a function of time, pharmacokinetic analyses can be undertaken to model how the CA distributes in the target organ, in order to obtain various vascular and extravascular parameters, which are expected to reflect tissue biology and pathology. This pharmacokinetic modeling is independent of the imaging conditions (MRI field strength) and in principle even independent of imaging modality (CT or MRI) [6, 11, 16, 17].

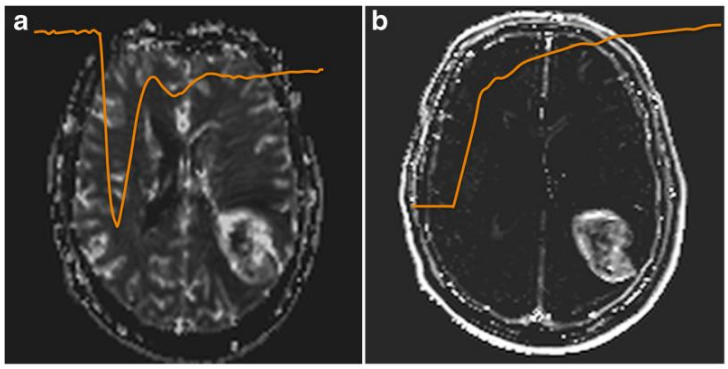

a – Cerebral blood volume map derived from DSC acquisition; Tumor signal evolution on DSC perfusion showing the negative curve due to the susceptibility effects of intravascular gadolinium; the second, lower, negative curve shows the recirculation effect; b – Ktrans map derived from Tofts extended pharmacokinetic model; Tumor signal evolution on DCE perfusion, showing the initial steep positive curve (due to the vascular enhancement) followed by the slower enhancement (due to the extravasation of gadolinium into the interstitial space).

Figure 17 – Perfusion-weighted imaging of a patient with left parietal glioblastoma

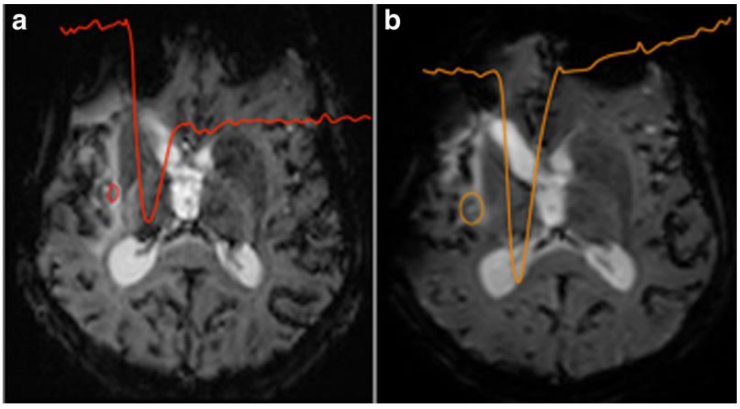

a – The gadolinium pre-bolus saturates the extravascular extracellular space; therefore, the DSC gadolinium does not present a significant leakage; b – Without previous bolus, the DSC gadolinium leaks into the extravascular extracellular space with significant competing T1 effect. Without correction of the leakage, the measurement of cerebral blood volume (derived from the area under the negative curve) is underevaluated.

Figure 18 – Perfusion DSC imaging of a patient with right temporo-insular glioblastoma: comparison of DSC acquisition with (a) and without (b) gadolinium prebolus.

Most models (Tofts, Tofts extended, adiabatic approximation of the tissue homogeneity model, the two compartment exchange model, Patlak, etc.) use the concept of compartments, i.e., intravascular and extracellular extravascular compartments, where gadolinium diffuses (gadolinium

does not enter into the cellular compartment). From these various models, the transfer constant Ktrans can be measured (see Figure 17). This constant characterizes the diffusive transport of Gd chelates across the capillary endothelium. It has been widely used to characterize tumor biology and treatment response. Consensus recommendations propose for the assessment of anti-angiogenic and anti-vascular therapies, Ktrans should be a primary endpoint. Secondary endpoints should include ve, the rate constant k ep (kep=Ktrans/ve), and the plasma volume vp (if available, according to the model used). The motivation for such advanced quantification of biomarkers is to address a limitation of current tumor response assessment methods (MacDonald, Response Assessment in Neuro-Oncology (RANO)), i.e., based on the diameter of contrast enhancement, that do not take into account the metabolic and vascular changes. An important requirement for the pharmacokinetic modeling is an accurate arterial input function (AIF) ideally derived from the same MRI data. In practice, this is often a challenge as a result either of the location of the target lesion or the measurement method used to acquire the AIF. Acquisitionrelated factors leading to poor AIF estimates include low temporal resolution (>3 s) per data sample, flow sensitivity of the method of acquisition and poor excitation, and saturation effects. As a result of these challenges, alternative methods have been proposed, among them the use of local AIF for DSC to reduce dispersion effects or a population-derived AIF for DCE-MRI or additional acquisition strategies employing a measurement of a pre-bolus using higher temporal sampling. A limitation for a wider clinical implementation of DCE MR protocols is the variability of the results according to the models and even to the software used [6, 11, 16, 17].

2.4.2 Arterial spin labeling

Arterial spin labeling (ASL) is a noninvasive MRI technique that does not require the use of any exogenous contrast agent. It uses electromagnetically labeled arterial blood water as endogenous tracer; hence, ASL can be used in all situations where the application of exogenous contrast agent or radioactive tracers is restricted. ASL allows quantification of blood flow in physiological units of milliliter per minute per 100 g, in brain and other tissues. Perfusion-weighted images are obtained by subtraction of labeled images (selective inversion recovery band applied below the imaging volume) from images acquired with control labeling (no saturation band applied below the imaged volume) as illustrated in Figure 19. After a certain post-label delay (PLD) superior to the bolus arrival time (or arterial transit time (ATT)), labeled images are acquired containing both labeled and relaxed water as well as static tissue water. A second experiment is then performed but without labeling, i.e., without selective inferior inversion applied prior to the image acquisition. The tagged region can be either a slab (PASL implementation) or a plane (pCASL, CASL implementa-

tions). In c, a saturation slab is added at time Tsat to precisely allows the sequence to control the bolus length.

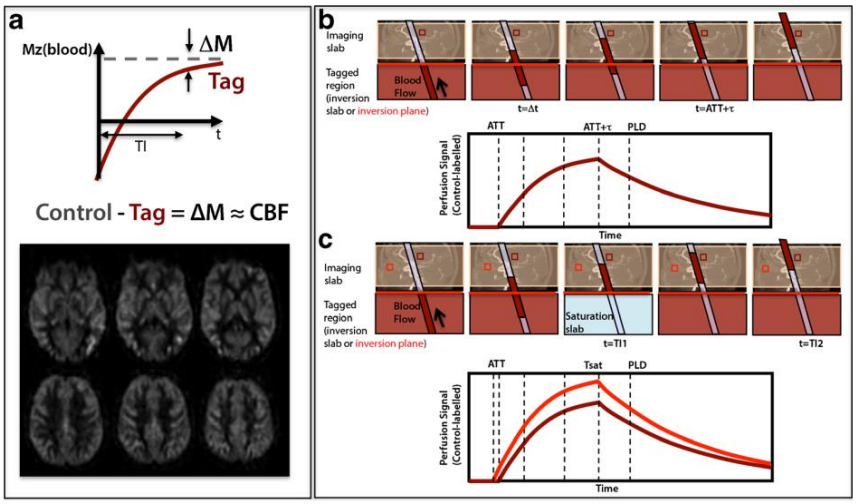

Figure 19 – The arterial blood water magnetization inverted by radiofrequency pulse a flows toward the image volume b while also experiencing longitudinal relaxation

The difference averaging are required to generate a perfusion-weighted image with sufficient contrast to noise. In practice, the number of measurements needed depends notably on sequence type (CASL, PASL, pCASL, etc.) and magnetic field strength, but an ASL acquisition typically involves 50–60 measurements. Consensus is emerging among the ASL community that the pCASL approach is the optimum labeling strategy that provides the best SNR due to longer tagged bolus duration (i.e., larger volume of tagged blood) and reduced T1 decay due to the inherently reduced time between inversion pulse and image acquisition. An extension of ASL consists in applying the selective inversion slab regionally in order to select one specific vascular bed territory, for example on the right or left carotid arteries. This figure also nicely illustrates the ability of ASL to detect acute stage hyperperfusion corresponding to luxury perfusion previously reported by PET studies. The presence of hyperperfusion on ASL-type perfusion seems indicative of reperfusion/collateral flow that is protective of hemorrhagic transformation and a marker of favorable tissue outcome. For image readout, three main sequences are currently being used in the literature: 2D EPI, 3D gradient and spin echo (GRASE), and 3D FSE with in-plane spiral readout. 3D imaging sequences facilitate the use of background suppression, a technique that suppresses the static tissue signal to reduce noise from motion and other system instabilities (Figure 20 and Figure 21).

Pitfalls. One difficulty with ASL in clinical routine is the intrinsic sensitivity of the technique to transit time effects, i.e., to the delay between the application of the tag and the arrival of the tagged volume. The ASL signal is exponentially dependent on the transit time, which in humans

is comparable to T1. This results in a compromise between short delay, i.e., reduced T1 decay, and optimal blood delivery to the tissue. Transit time is reduced with CASL and pCASL, and to circumvent the problem in PASL, saturation pulses can be applied to the tagged volume, starting at a time Tsat, that should be inferior to τ, the temporal length of the tagged bolus, further allowing one to also precisely define the bolus duration. Added to this difficulty is the sensitivity of the ASL perfusion signal to heterogeneous ATT. The ATT is strongly variable between subjects; it varies regionally between territories, depending on the pathologies, and can be substantially prolonged in some neurovascular diseases such as proximal vascular stenosis at the level of the ICA but also moyamoya disease. In such cases, the estimation of the ATT providing the hemodynamic information in each pixel is mandatory, leading to the concept of multiple postlabeling delay (PLD) acquisitions. Finally, because the ASL signal is small and requires signal accumulation, motion and other instabilities can degrade the perfusion images. State-of-the-art implementation of ASL includes a motion co-registration of images prior to subtraction and averaging. Background suppression may further improve sensitivity and reproducibility [16, 17].

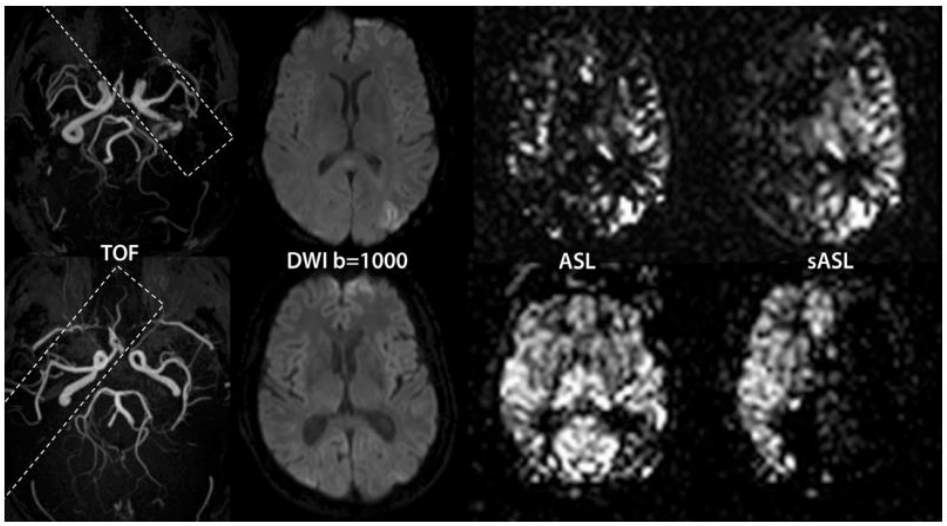

Figure 20 – Difference between selective ASL (sASL) and nonselective ASL in two different patients. The dotted rectangular line shows the volume of the radiofrequency pulse stimulation. Note in the first patient (upper row), the increase of perfusion on the ischemic lesion, corresponding to the luxury perfusion

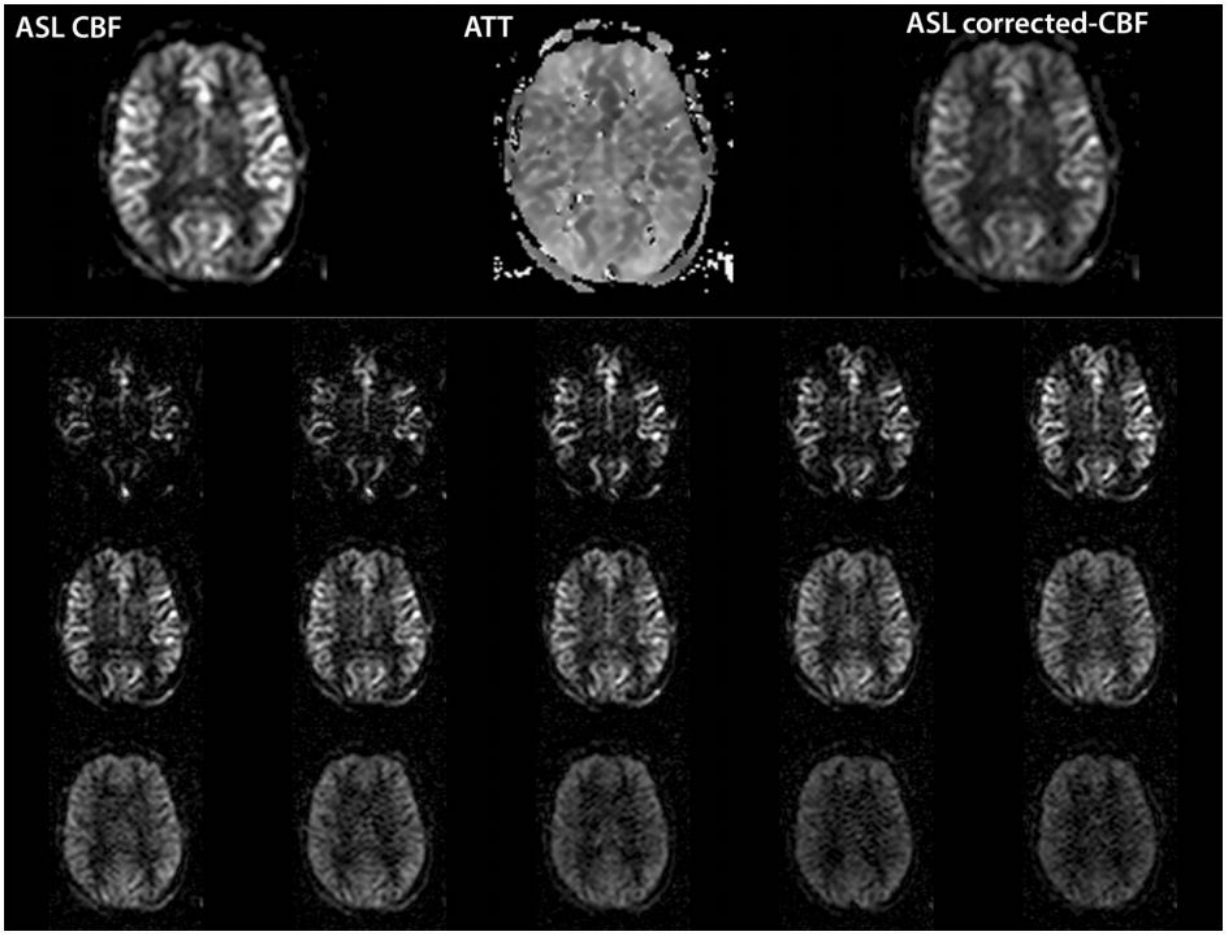

Figure 21 – 3D GRASE sequence with multi-time post-labeling. First line shows non-corrected ASL single labeling time (TI= 2,200 ms) CBF map, ATT maps, and ASL corrected CBF map

2.4.3 Presto

The presto sequence was developed as a functional imaging technique in the early days of fMRI. The name stands for 'Principles of Echo-Shifting with a Train of Observations', referring to two of the most significant features of the sequence, echo-shifting and a multi-gradient echo type acquisition, as is used in interleaved echo planar imaging (EPI). In the first experiments using bolus tracking, it was realized that accelerating the scan by shortening the TR severely restricted the range of available echo times (TE's), which could be detrimental for optimal contrast for the T2 effect of the bolus; this problem was minimized by shifting the echo towards the end of the TR interval. As it is written in that paper: "MR images were obtained with an unmodified 1.5 T unit (GE Signa) by means of a fast GRASS sequence, with the echo shifted towards the end of the repetition period by means of an increase in the readout dephasing gradient, this increase produced a repetition time of

16 ms and an echo time of 12 ms……" (the length of the dephaser effectively controlled the delay between excitation and acquisition). It was essentially this push towards longer TEs, together with the restriction on the repetition time of the sequence related to the desired spatial resolution and image-to-image time resolution, that led to the idea of delaying the echo into a subsequent TR period, resulting in a TE longer than the TR of the sequence. This idea was called 'Echo Shifting' (ES). The first implementation is shown in image below, with the gradient waveforms modified and added to refocus the signal from each RF pulse after the subsequent one. The modifications entailed: refocusing of the readout gradient in each TR, moving the phase encoding to the end of the TR period, and changing the slice select gradient to a +1/2, +1, -1 scheme where '+1' refers to the surface area (time integral) of the slice select gradient used during the RF pulse. Crushers were added (the line 'Gadd2') to further suppress the signal directly after the RF pulse. This additional gradient was reversed in the next TR to refocus the desired signal. This scheme was generalized to an arbitrary number of TR shifts by changing the slice select gradient to a 1/2(n-1), +1, -1 shape and the additional gradient to step through a cycle of n-values; an example for a three cycle scheme for a 2 TR shift is shown in line "Gadd.3". While first implementations were done on a 4.7 T animal scanner and demonstrated with bolus tracking on a cat, subsequently the echo shifting method was ported to a clinical scanner for fMRI with bolus tracking in humans. The ES-FLASH acquisition was then accelerated by using multiple readout echoes within every TR in an interleaved EPI fashion, creating the PRESTO sequence (Figure 22).

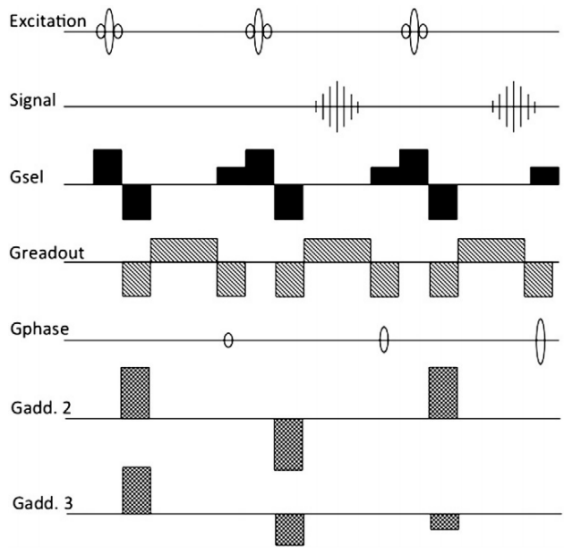

Figure 22 – First two implementations of the Echo Shifted gradient echo imaging. 'Gsel' is the slice selection gradient, 'Gadd' the additional gradient used for shifting the echoes, shown in two versions (2 and 3), see text for more details

The first implementation used just the slice select waveform to de- and rephrase the desired signals. It was a 2D, single slice sequence, again demonstrated with bolus tracking in a cat brain. With a TR of 9 ms, a TE of 13.5 ms, a 64×64 image was acquired every 153 ms. The next step came with an improved scheme for the additional gradients in an ES-FLASH implementation on a clinical scanner. This was the first time echo shifting was applied to fMRI, requiring a change in the gradient scheme to improve the temporal stability. The new scheme allowed for an arbitrary number of TR shifts while keeping the same waveforms for every TR period. This was achieved by using two crushers in every TR, one before and one after the acquisition, with a ratio of 1:2 for a shift of one TR. It can be generalized to a ratio of n:(n+1) to shift over n TR periods. The slice select gradient was still used as well for the echo shifting, similar to the previous implementations. Also the phase encoding was rewound in every TR to keep the gradient moments constant, improving the stability. Two other additions brought this closer to the final PRESTO version: the extension to 3D encoding and the use of phase scrambling to improve suppression of stimulated (RF) echoes. This suppression again was essential to improve the stability for the fMRI application. The method was used this time for BOLD contrast fMRI with a visual stimulus. A 30 ms TE was used, with a 20 ms TR, resulting in a 20 s 64×64×16 volume acquisition time. The final version came out a year later, final at least in the sense that this is more or less the sequence that we now understand to be PRESTO. It combined the 3D phase encoding with the multiple echo acquisition and echo shifting from the previous version. It also had the additional gradient design from the previous 3D ES-FLASH method, as well as its phase scrambling. One small difference is that now the slice select gradient is finally completely separated in function from the echo shifting additional gradients, the -1:2:-1 design will refocus both the signal from the current excitation as well as the preceding ones. This implementation acquired 5 echoes per 24 ms TR, a TE from 30 to 40 ms, for a 64×50×24 voxel volume every 5.8 s. One more technical detail of interest for PRESTO is the choice of the phase encoding order over the echoes within one TR and over subsequent TR periods (Figure 23 and Figure 24). This choice affects the nature of the EPI type artifacts (ghosting and distortion) stemming from the alternating sign of the readout gradient and the different T2 weighting and phase accumulation for the different echoes within one TR. Our choice in general has been to make the steps between the echoes in one TR (the ‘blips’) large, and fill in the intermediate lines in subsequent TRs (Figure 25).

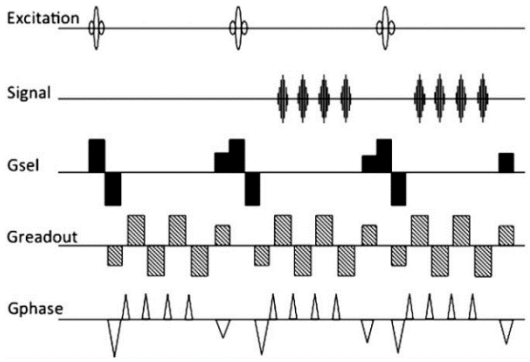

Figure 23 – The first PRESTO sequence, combining the echo shifting with multiple readouts per TR

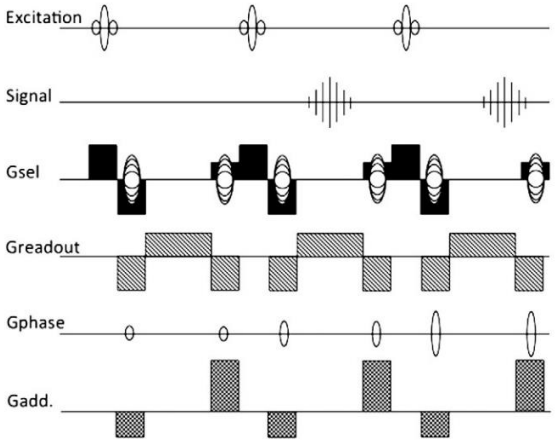

Figure 24 – Echo shifted FLASH with an improved gradient design and 3D encoding

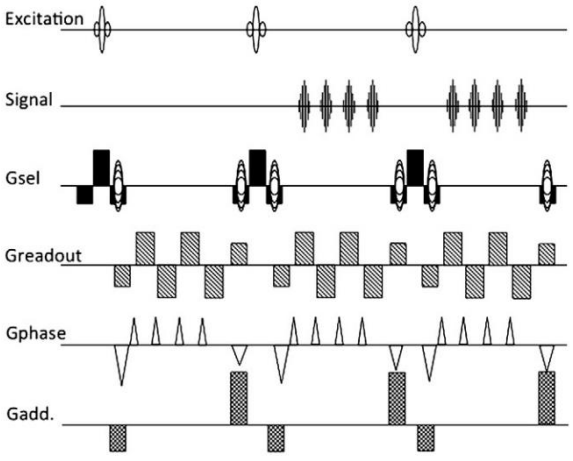

Figure 25 – The PRESTO sequence in its final form: 3D encoding, with multiple echoes per TR period and additional gradients to shift the echo time beyond the TR time

On figure 26 a patient with a left-frontal glioma was scanned to localize the language areas to inform the neurosurgeon. Shown are 9 slices of a PRESTO experiment with 2D SENSE and 8-channel headcoil on a Philips 3 T. Images are of language task (verb generation) in a patient with a left frontal glioma, used for surgical planning. Scan parameters PRESTO: TR 22.5 ms; TE 33.2 ms; echo-shifting of 1 TR; flip angle=10°; FOV 224×256×160 mm3; matrix 56×64×40; voxel size 4.0 mm isotropic; 0.6075 s per volume; 40 slices; sagittal orientation. Activity exceeding a statistical threshold is projected onto a FLAIR scan which shows the tumor, and on a T1-weighted anatomical scan. In this case the frontal language area (Broca's area) was immediately posterior to the tumor (yellow arrow in figure), prompting the surgeon to perform awake surgery involving electrical stimulation to avoid damaging that region. Improvements in gradient performance to 22 mT/m amplitude and 115 T/m/s slew rate allowed for a speed up of the PRESTO sequence to make 3D bolus tracking feasible in 2000 (with 64×52×32 resolution in a 2 s volume TR) and similarly on a clinical Philips scanner. Apart from bolus tracking, PRESTO has also been applied to T2* contrast based anatomical imaging. The addition of a navigator echo improved the stability and with it the detection sensitivity, as some of the signal fluctuation inherent to multi-shot acquisition can be corrected for by compensating the shot-to-shot amplitude and phase variations [16, 17, 18].

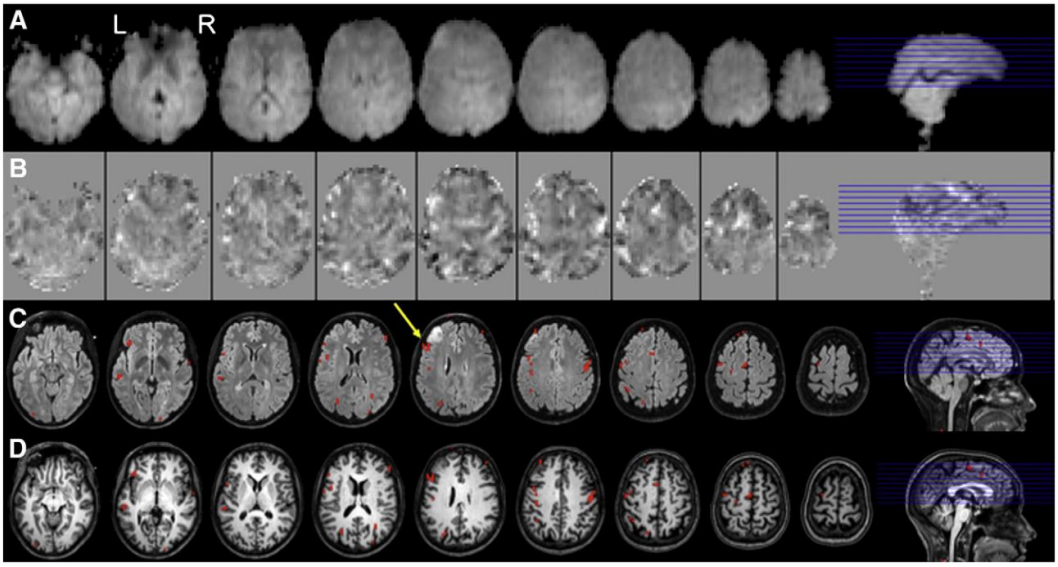

a – average PRESTO scan; b – T-maps of language activity (range -10 to 6); c – activity exceeding a threshold of t=5 (pb0.05 Bonferroni-corrected) projected onto a FLAIR scan; d – same on T1-weighted anatomical scan.

Figure 26 – Demonstration of the localization of Broca's language area in a candidate for surgical resection of a brain tumor using PRESTO fMRI

In order to find the right sequence to visualization of vestibular system, we started to use different sequences using volunteers.

3 Experiment planning and results

The studies of anatomical structure of inner ear and blood flow planned. Some studies will be done in Tomsk region in "MRT-expert" company and some of them in an Ultra-High-Field MRI centre Scannexus as a part of Maastricht University.

The daily routine programs will be used – T1, T2, Drive. Space, Stir, TOF, ASL pcals, Presto, Mprage,

This programs are available in different in all scanners, and can be used in daily routine practice.

3.1 Experiment planning

3.1.1 General information

The temporal bone has a highly complex anatomical structure, in which the sensory organs of the cochlea and the vestibular system are contained within a small space together with the sound-conducting system of the middle ear. As known, the inner ear consists of cochlea, superior, posterior, horizontal canals, endolymphatic sac, saccule, utricle, Cochlea, ductus reuniens, utricular and sacullae maculae, crista ampullaris and fluids in the inner ear canals. Malformation of these compartments of inner ear can play tremendous role in the disease development such as Benign paroxysmal positional vertigo (bppv), ménière's disease, hearing loss [1]. Fluid disturbances in the inner ear represent a special medical challenge to otolaryngology and oto-neurology. The two inner ear fluids, perilymph and endolymph, play a critical role in inner ear homeostasis, and anomalies in the compartments containing these fluids may be associated with auditory neuropathy, acute peripheral vestibulopathy, neurovascular cross-compression, and endolymphatic hydrops or Meniere's disease. Moreover, the inner ear has a complex system of blood flow also. It is principally supplied from the inner ear artery (labyrinthine artery), which is usually a branch of the anterior inferior cerebellar artery. Cochlear blood flow is a function of cochlear perfusion pressure, which is calculated as the difference between mean arterial blood pressure and inner ear fluid pressure. Thereby, impaired blood flow and malformations of endolymph and perilymph fluids make an additional contribution to diseases development. The human vestibular system is not easily accessible for investigation because this delicate sensory organ is hidden deep in the temporal bone [2].

Understanding the parameters of blood flow, homeostasis and building a fully detailed anatomical structure of inner ear is a key to success in developing targeted pharmacological and surgery invasions in order to eliminate the diseases [4, 3].

Structure of the fine osseous anatomy of the inner ear can be obtained using modern computed tomography (CT) scanners and cone beam CT (CBCT). Analysis of the soft-tissue constituents of the labyrinth, however, is beyond the scope of X-ray techniques. Both in the present and in the near future, anatomical structure of the membranous labyrinth can (at best) be expected from magnetic resonance imaging (MRI). Contrast-enhanced magnetic resonance imaging (MRI) has become a frequently used clinical tool for diagnosis and examination of pathophysiology of inner ear and retrocochlear abnormalities. Currently, anatomical structure of the membranous labyrinth in the clinical setting remains a challenge despite significant technological advances. [1].

Despite tremendous advances in magnetic resonance imaging protocols in recent years, the ability to image finer details of membranous anatomy of the inner ear still lies in the domain of ultra-high-field magnetic resonance imaging (UHF-MRI) scanners, defined here by a field strength equal to or greater than 7 T. Detailed clinical imaging of membranous components of the inner ear remains elusive because of the inability standard programs of commonly-available 3 T scanners to image the inner ear at adequate resolutions.

Several MRI research centers have attempted to visualize inner ear anatomy at 7 T, with varying degree of success. Structures such as the osseous spiral lamina and the labyrinthine artery can be visualized at 7 T, but the scala media and its boundary structures are indistinct or blurry at this field strength. The anatomy of the otoliths has been studied, but there is limited information regarding their supporting connective tissue structures such as the membrana limitans in humans [5].

Therefore, it remains an unsolved problem for a medical community, and the detailed understanding of the deep relations of the footplate is crucial to assess the risks and outcomes of different intervention.

For this reason, the size baselines of the inner ear compartments will be collected using MRI in our study. Moreover, we will try to detect perfusion of inner ear. The results of current investigation will make possible to assess the malformations of the inner ear compartments and to determine the blood flow in the inner ear and its volume.

The studies will be carried out with contrast agent in strict compliance with the rules of the Scannexus center and “MRT-Expert” indicated on the official website of the center: https://scannexus.nl/information/documentation, http://www.mrtexpert.ru

3.2 Study design

Objective: Anatomical structure assessment and perfusion detection of human vestibular system using Magnetic Resonance imaging.

Study design: Observational study

Main study/parameters endpoints:

Anatomical structures assessment and blood flow perfusion detection with and without the preliminary injection of contrast.

Nature and extent of the burden and risks associated with participation, benefit and group relatedness:

First, volunteers fill a written informed consent form out, followed by filling out a questionnaire (Safety scanning form) which is routinely done in Scannexus and MRT-Expert covering the following items: the presence of pacemakers, brain surgeries, heart rhythm disorders, claustrophobia, pregnancy, acute renal injury, allergic reactions, using medical plasters that cannot be taken of and different metal inclusions such as: metal objects in the body, piercing, jewelry, tattoos, permanent make-up. Then the scanning itself is performed. The complete procedure takes on average about 1 hour. This diagnostic procedure is used around the world with great success without restrictions. There are no risks related to the standard procedure of magnetic resonance imaging.

1. Introduction and Rationale.
2. Objectives:

2.1. Assessment of the anatomical structure of Vestibular system using Magnetic Resonance Imaging 1,5 and 3.0 with and without the preliminary injecting of gadolininium-containing contrast agent – Gadovist:

2.2. Vestibular system blood flow perfusion detection using MRI specific methods – Presto and ASL methods.

3. Study design: Observational study.

Duration: 3 months (01.08.2019 – 01.10.2019)

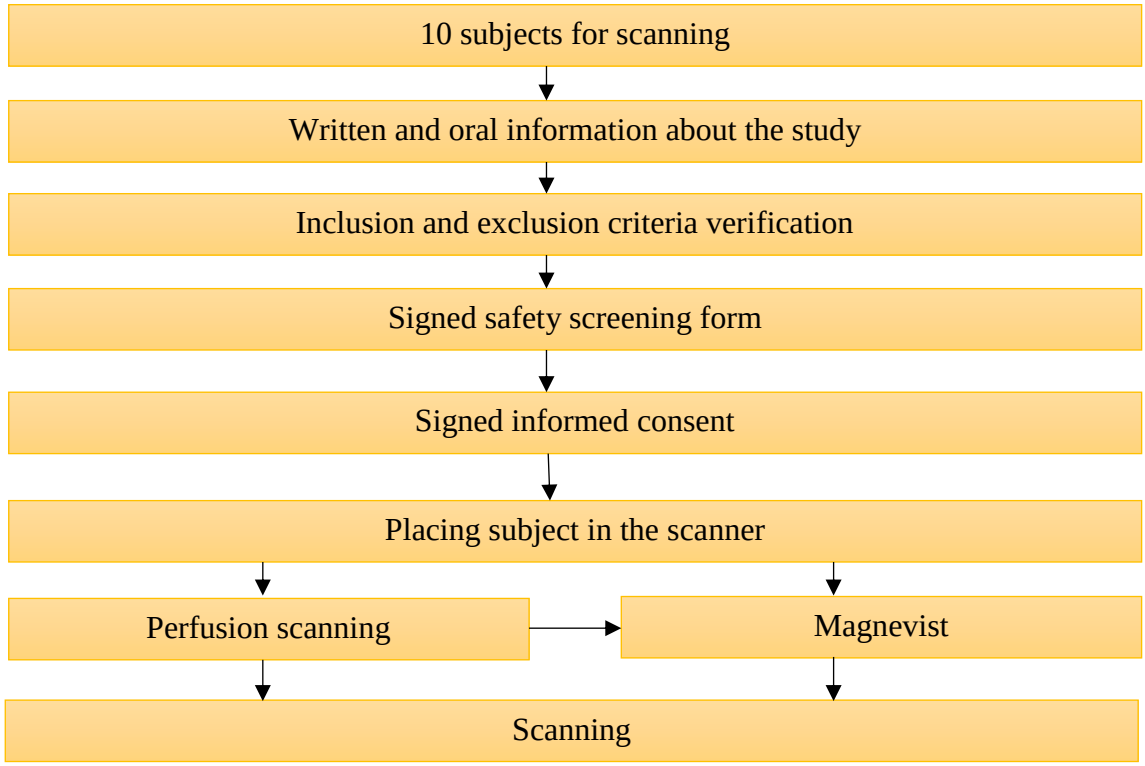

4.1. Population base: 10 healthy people 18 – 55 years old.

4.2. Inclusion criteria:

– Adults people (>18 years old);

– No match with any of "Exclusion criteria" (3.3);

– Signed informed consent;

– Filled the questionnaires (Safety screening form MRI).

4.3. Exclusion criteria:

– <18 years old;

– the presence of an active implant (pacemakers, neurostimulators, insulin pumps, ossicle prosthesis, or residual leads).

Foreign objects (dental fillings, metal dental implants, crowns, clips on blood vessels, metal splinters in the eye or body as consequence of shooting/accident/metal worker, orthopedic implants, braces, metal wire behind the teeth, mechanical contraception spiral and other things that cannot be taken of: Piercings, tattoos, permanent eye make-up medical plasters (e.g. nicotine))

– Cardiovascular diseases

– the presence of tumors and other diseases which affect to the results of the study

– Head and brain surgery

– Epilepsy

- Heart rhythm disorder
- Circulatory problems
- Claustrophobia
- Pregnancy
- Allergic reactions and risk of anaphylactic shock
- Acute renal injury.
- Incapacitated patients
- Refusal to fill out informed consent or Safety screening form MRI

4.4. Sample size calculation

As this is an observation study, the sample size is based on a current estimation of healthy people that want to volunteer now

4.3. Main study parameters/endpoints:

The anatomical structure of vestibular system will be observed in this study. The main end-points are: presence of all compartments of vestibular system.

The perfusion of inner ear tissues should be detected.

4.4. Withdrawal of individual subjects

There are some withdrawals of individual subjects from the study:

a) no signed informed consent of patient;
b) no signed questionnaires;
c) allergic reactions after intravenous administration of Gadovist;
d) claustrophobia in scanning session;
e) fatigue during the scanning;
f) pains of different etiologies during the scanning;
g) need to go to the toilet during the scan.

4.5. Premature termination of the study:

a) claustrophobia in scanning session;
b) fatigue during the scanning;
c) pains of different etiologies during the scanning;
d) need to go to the toilet during the scan.

3.3 Study procedures

In our study, each subject will be examined by the 1,5 Tesla and 3 Tesla MRI scanners. The study will be performed with and without contrast-containing agent Gadovist.

A contrast injector (Acist and Bracco) is available. To administer intravenous contrast to the subject a medical physician will be invited and a special procedure will be followed. The dose of Gadolinium containing agents (Gadovist) will be administered intravenously as a bolus injection.

The introduction of gadovist and its storage is carried out according to the rules of the manufacturer specified in the registration documents (link: https://pharma.bayer.nl/nl/geneesmiddelen/gadovist-10/).

The study will be performed in Scannexus and MRT-expert.ru in accordance with standard operation procedures of daily routine practice. Standard Operation Procedures (SOPs) published on the official web-site of the Scannexus centre (link: https://scannexus.nl/information/documentation, http://www.mrtexpert.ru).

The researcher will inform the subject about the study and ask to fill out and sign a questionnaire (Safety Screening form, Appendix 1 of Master thesis). After that, the informed consent should be signed.

The researcher will explain the Experiment. One does not need special preparation when having an MRI scan. It is recommended to wear comfortable clothing without metal buttons or zips.

A medical physician will be present during the scan session for contrast injection. The support staff member will know the procedure of inserting an IV cannula and will work according to this procedure. He/she knows how to use the contrast injector and how to administer the contrast agent to subject. He/she is familiar with the Scannexus emergency procedures.

There are two procedures: Setup the contrast injector with contrast agent and NACL, Inserting IV cannula to subject

When medical physician will Setup the contrast injector with contrast agent and NACL, he will make sure that all air bubbles are removed in the system, will select the program needed in the remote control.

The physician will wear gloves while inserting the IV cannula, disinfect skin with disinfectant, Insert the infusion needle, check the position of the cannula. Once blood will be visible in reservoir of cannula, the physician will remove the needle, connect cannula to extensions set + NACL prefilled syringe/ or directly to connecting tube of contrast injector, will Fixate the cannula with an infusion patch to the arm, flush with NACL to see if cannula and vein is open, will check once again if all the air is expelled of the contrast injector, and then connect the intermediate tube to the infusion needle, will start the pump to administer NACL drop by drop, to keep the vein open.

The subject will lie down on the research bed that will be moved into the scanner's tube which has a diameter of about 60 cm. During the scan patient body will be (partly) inside of the tube. When patient is in the scanner, a few images will be acquired. While scanning, the scanner

regularly produces a knocking or ticking sound. This is normal and is required for producing the images. If it necessary, during the procedure, patient can alarm the researcher by squeezing a ball. During the scans, the researcher will be outside the scanner room, but will be observing the tested subject at all time to make sure that the patient is fine. For the quality of the images it is important to stay as still as possible in the scanner during the procedure. The magnetic resonance imaging research will last no more 60 minutes.

As far as known, the magnetic field and radio waves being used in magnetic resonance imaging do not result in harmful side effects.

All measured MRI data (dicom) is automatically stored to the Hard Drive of Syngo system (Dicom Images storage) in Scannexus centre. In MRT-expert we will use Synergo Hardware system.

3.4 Contrast – containing agents

Magnetic resonance imaging (MRI) contrast agents are widely used to increase the contrast difference between normal and abnormal tissues. The signal intensity of biological tissues in MR imaging depends on the relaxivity of water protons, reflected in tissue-specific values of T1, T2, and T2*. Shorter T1 relaxivity causes an increase in signal intensity, whereas shorter T2 relaxivity causes a decrease in signal. GBCAs are strongly paramagnetic and shorten the T1 and T2 relaxivity of adjacent water protons, which results in an increase in signal intensity on T1-weighted images, and a corresponding decrease in signal intensity on T2-weighted. Gadolinium has a more pronounced effect on T1 relaxivity, and therefore its impact on signal intensity is most pronounced on T1-weighted images.

In spite of the main goal is to detection anatomical structure of the vestibular system in daily routine practice the radiologist, we choose the most common contrast containing agent – Gadolinium sodium. It will be Magnevist and Gadovist. The procedure of storage and injection will be performed in accordance with the standard rules of Manufacturer. The allergic reaction can be present during the study. The medical doctor who can operate anaphylactic shock included as a part of project team.

3.5 Equipment and programs

We will performed the studies using two different scanners. One of them is a Philips Intera 1,5 Tesla scanner which located in Tomsk region. The other one is Siemens Magnetom 3 Tesla scanner which located in Maastricht university.

Although it's the scanners from different manufactures the uniform approach and the uniform programs are present.

For a scanning we need to start with localizer. In philips scanners It's survey, in Siemens is localizer. It necessary to excite Hydrogen atoms in certain part of body. In our examples It's a brain with focusing in the innear ear.

Since we decided that it's necessary to assess inner ear in daily routine practice, we will use only standard programs which preinstalled in each MRI scanner.

In our study, we are trying to choose appropriate sequences for future research. Thus main programs will be selected such as: T1 and T2 relaxation, SE, TSE, multi speed TSE (Drive and Space), gradient sequences, Flair, DWI, TOF, MPrage, perfusion sequences (Presto). We know that the average time in daily routine practice is 15-25 minutes for a brain and 15 minutes for a vessels.

For accident detection, It's necessary to choose the appropriate parameters for radiologist. We decided that vosel size will be 0,3mmx0,3mmx0,3 mm with 1mm slices. In case of good results of study it can be performed with less size of voxel.

TR and TR will not the same for different sequences and different MRI scanners.

3.6 Results of studies

The subjects were assessed. For patient safety, we include one subject to one research. Research results and discussion.

First of all we performed the daily routine studies of brain assessment using the simple sequences – T1 and T2 relaxation. It was done without contrasting and focusing on the inner ear. In Figure 27, you can see the sequence T2 relaxation. As a results, It possible to separate white and grey matter of brain, to assess osseous structure of brain effectively. The middle ear not clearly visible, but innear ear not available. It's not possible to assess vestibular system.

The figure 28 shows us the T1 relaxation with contrasting by Magnevist. As we discussed before, the bone structure preferable assessed using the T1 relaxation and we thought that is possible to see the vestibular system in brain observation study. But as we can see from the result, there is no information about the inner ear.

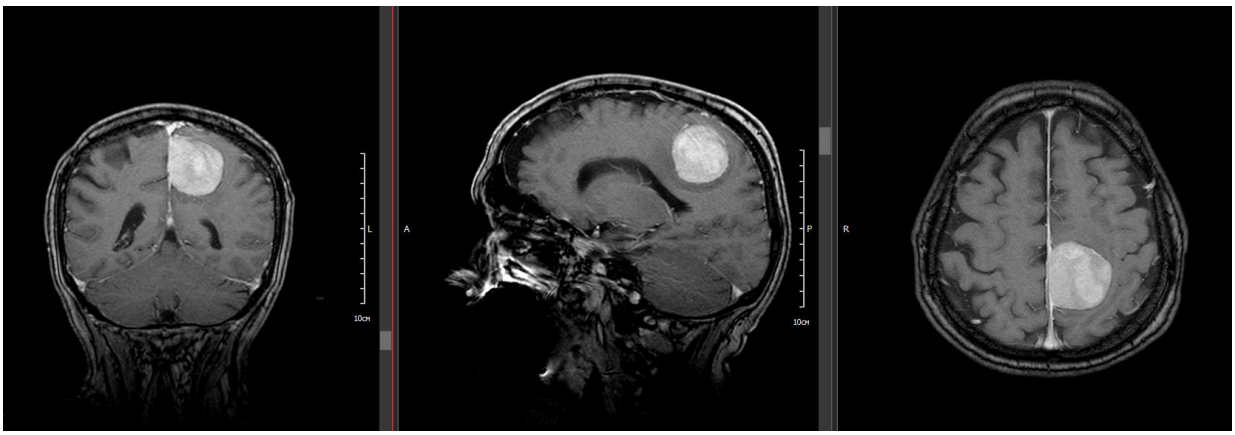

a. b c.

a – frontal plane; b – sagittal axis; c – axial axis.

Figure 27 – The T2 relaxation without contrasting

1. Next step. We tried to increase signal and applied the contrast containing agent – Magnevist. The Physical parameters were not changed and parameters from study no. 1 were used. TI, and TE were the same as mentioned in study №1.

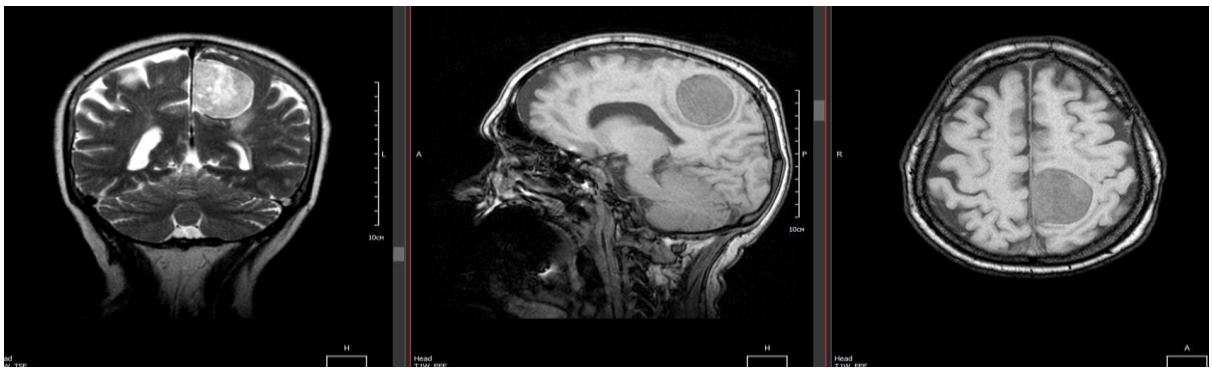

a. b. c.

a – frontal axis; b – sagittal axis; c – axial axis.

Figure 28 – The T1 relaxation with contrasting

In order to start the perfusion study, we should detect the vessels of brain and Willis circle. As we know from the Radiology and Physical principles of MRI, MRI is the only tomographic method which allow to see the blood flow without contrasting (Figure 29, a). And we made sure there are no differences in comparison with contrasting (Figure 29, b). It was applied the Time-of-Flight method which described in other chapter of this Master's thesis.

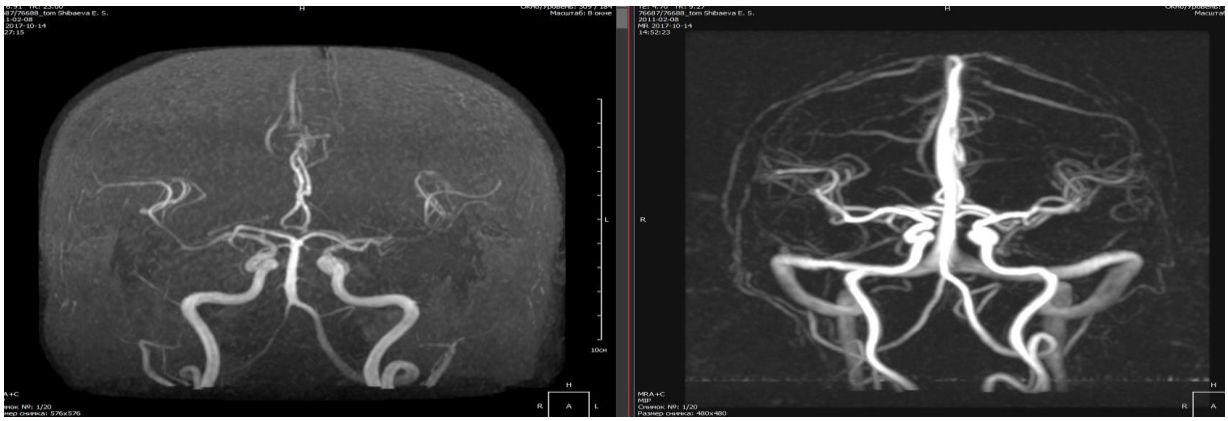

a. b.

a – before contrasting; b – after contrasting.

Figure 29 – The blood flow assessment using TOF protocol

Discussing about future studies we decide to choose different sequences. We knew that the inner ear is liquid-contained structure and can give signal both T1 relaxation and T2 relaxation. In order to take the high fast signal we add FFE gradient sequence which is to take place with T1 relaxation and Fast Advanced Spin Echo sequence which work in T2 relaxation.

In order to take the images of inner ear the high-resolution new sequences were practiced. We choose the sequences “Drive” which refers to Accelerated spin-echo relaxation with an equilibrium angle of 90º. The Fast Advanced Spin Echo (FASE) sequence uses a ETL of 212 in the sequence. This results in an extremely short scan time. In addition, half Fourier Imaging (HFI) imaging is used here. The combination of 212 echoes and HFI leads to scan durations, which are only a small part of the scan duration in a normal SE sequence. Each echo from this sequence with 212 ETL fills one line of k-space. K-space fills up a bit more than 50%. Initially, the method used as a multi-slice was used to reduce the scan time, but data collection with a normal SE (spin echo) T2 sequence reaches 20 minutes. During this time, a practical problem arises: the movement of the patient. It is very difficult to lie still for such a long time.

We also used fast low angle shot (FLASH, FFE) is the most commonly used gradient spoiled gradient-echo MRI-sequence. FLASH uses radio frequency excitation pulses with a low flip angle (less than 90 degrees) and subsequent reading gradient reversal for producing a gradient echo signal. The small flip angle pulses create equilibrium of longitudinal magnetization. Transverse magnetization is eliminated by a strong gradient (spoiler gradient).

As you see in Figure 30 the best signal we take from the T2 Drive sequence. Seemingly It’s connected with the liquid in the inner ear. The T1 FFE have a low signal, It can be changed using

the higher resolution. But the increasing the resolution will require an increase in scan time. The Flair didn’t gave result due to the absence of acute inflammation in the inner ear.

a.

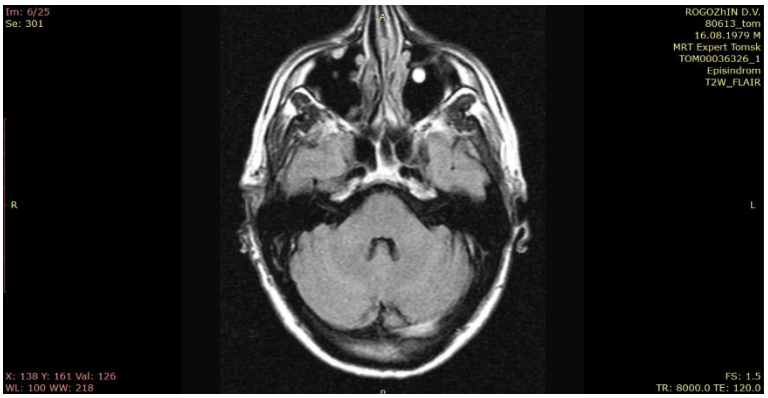

b.

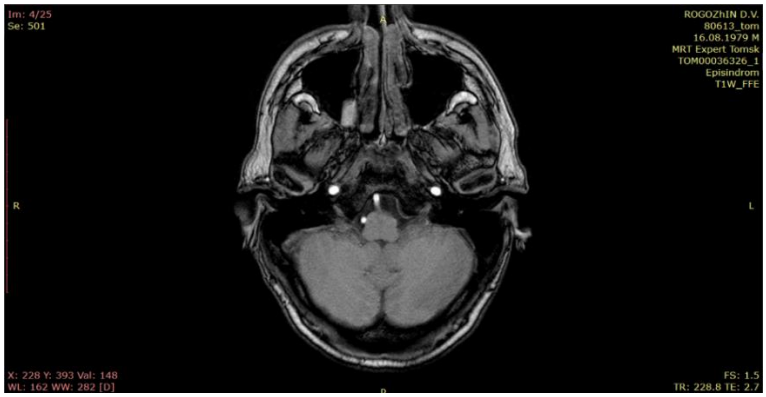

c.

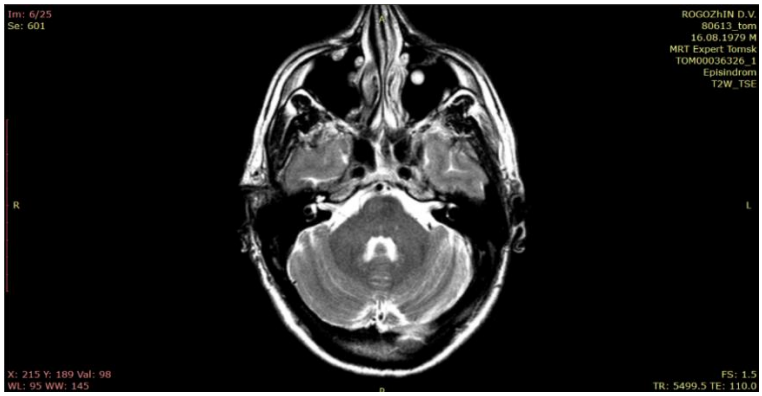

d.

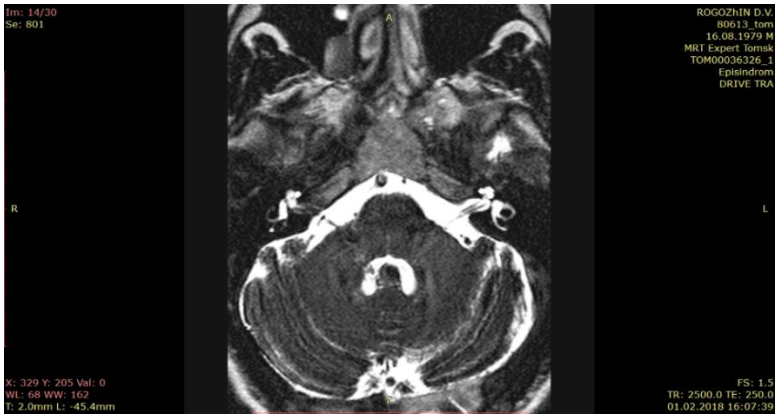

a – T2 Flair, b – T1 FFE; c – T2 TSE; d – T2 Drive.

Figure 30 – The inner ear assessment using 1,5 Tesla MRI scanner

Now, we understand that It possible to see the innear ear using 1,5 Tesla scanner playing the physical parameters (TE and TR).

But It's not enough to understand pathophysiology and etiology some mentioned disease such as: Meniere's disease and BPPV. In future, we must separate all compartment of the innear ear in order to deeply understand the disease development.

This way, we decided to repeat our results using 2 Tesla scanners.

First of all, we repeated standard sequences T1 and T2 relaxation. We understood that there no difference between 1,5 and 3 Tesla scanners (Figure 31 and Figure 27-28).

Next step, we tried to used T1 inversion recovery sequences MPrage and T2 Space in Siemens 3 Tesla scanner as analog of T2 Drive in Philips scanners.

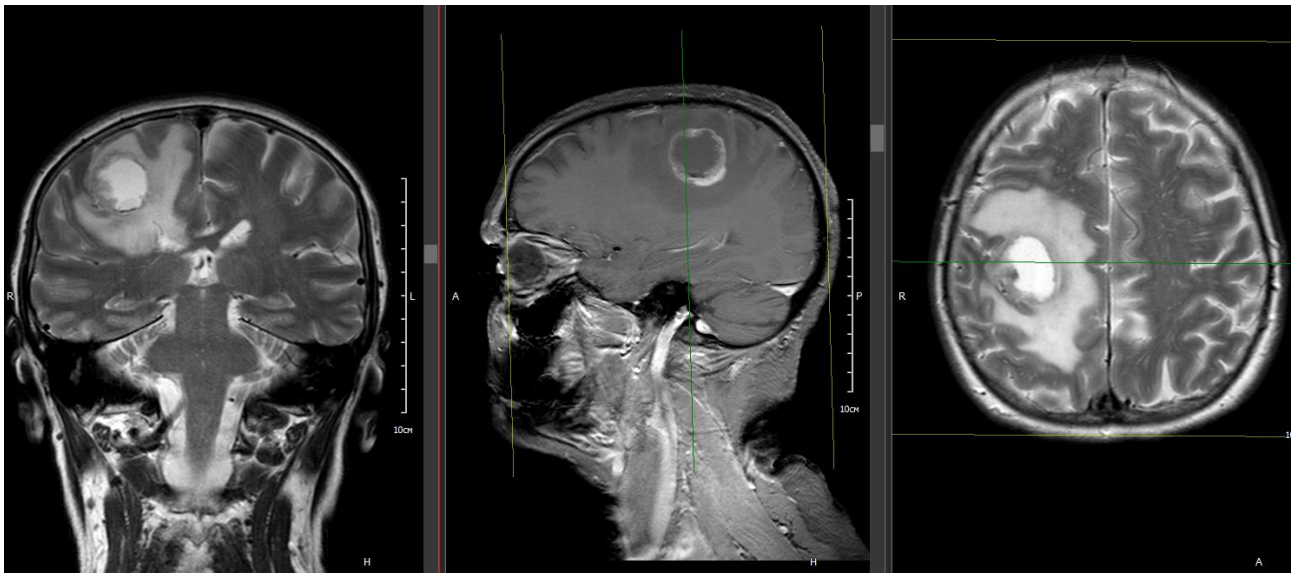

Frontal axis Saggital axis Axial axis

Figure 31 – The T1 relaxation using 3Tesla Siemens scanner

To obtain high-quality images, the task was to set up superfast sequences. The T1 tse sequence was used, which is a multi-echo spin-echo sequence, where different parts of the k-space are recorded on different spin-echoes. A spin-echo sequence with four echoes in which TE equals 15 ms. The advantage is that the image can be obtained four times faster. As we can see in the example, on T1 TSE, the image of the inner ear and nearby tissues is not clear.

T2 Space (3d accelerated spin-echo sequence) - Spin-echo sequence - Very gives a very strong signal and shows a small number of artifacts. Clear image of the inner ear.

T1Mprage - MPRAGE is a modified TurboFLASH series with preliminary magnetization of inversion pulses. When acquiring images, a 180-degree primary pulse inversion is used, followed by a sequence of gradient echo signals that form an image (steady state using rewind gradients). To

obtain a 3D image, the secondary phase is encoded in the direction of the selected slice. Only one segment or section of 3D data recording receives a preliminary impulse. After receiving the signal from all lines within the 3D image, the delay time TD follows. the sequence did not allow to detail the structure of the inner ear.

a.

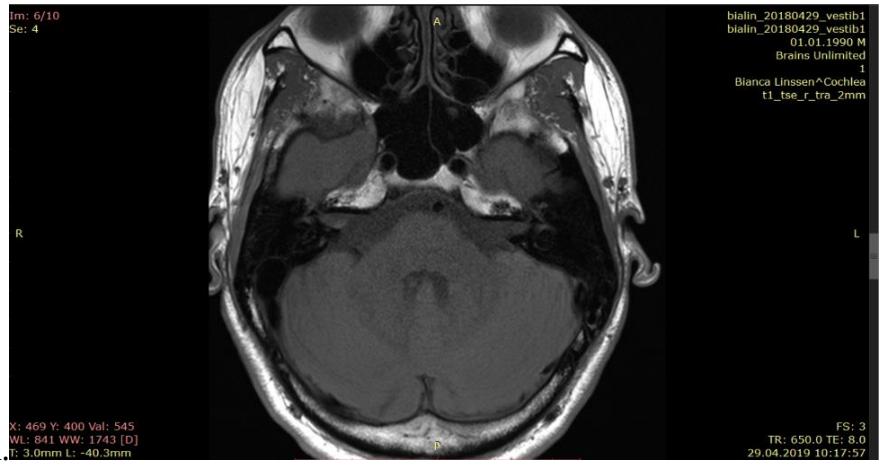

b.

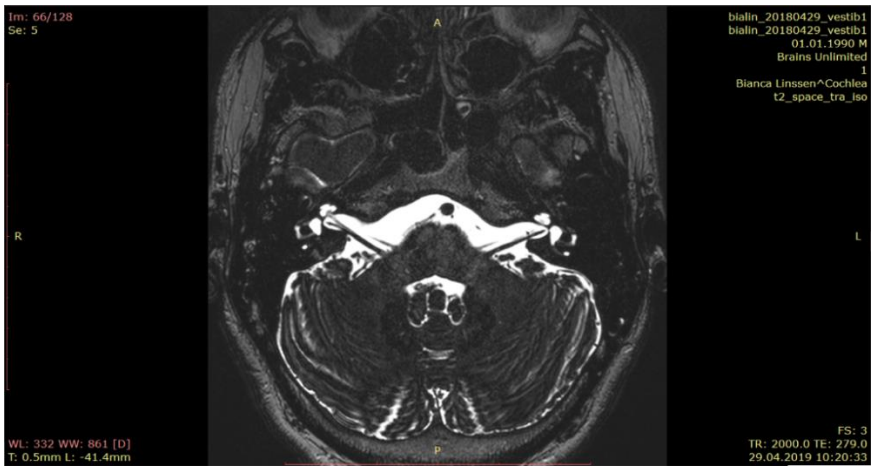

c.

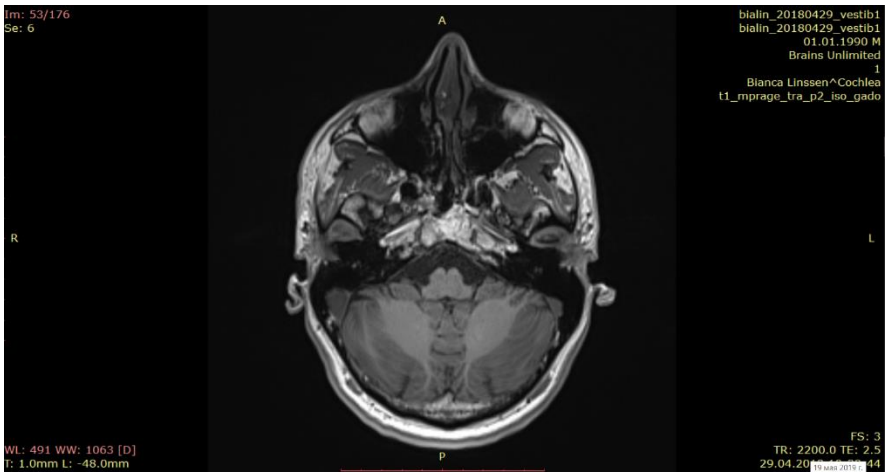

a – T1 TSE; b – T2 – Space; c – T1 MPrage.

Figure 32 – The vestibular system assessment using 3Tesla Siemens scanner.

As mentioned before, we used on 3Tesla scanners the same parameters as 1,5 Tesla. The all parameters you can find in Appendix 2 of Master's thesis.

Briefly speaking about perfusion, we found only available method on 1,5 Tesla Philips scanner. It was Presto method. The main purpose in this study is to detection of perfusion. As known, the perfusion methods such as Presto, DCE and DSC are perfumed using contrasting. But there a lack information about the human blood flow in the inner ear. And now, It's necessary to choose right physical parameters for future studies. Moreover, there must be a delay before scanning by reason of the contrast is injected to the arm vein. We know that the time of the great circle of blood circulation is 23-27 seconds and it takes time to reach the inner ear. This reason, two techniques were used to detect perfusion. Both methods are the introduction of a contrast agent with a delay before the start of the scan. In the first case, we used a delay of 15 seconds. In the second case - 5 seconds.

To exclude the influence of various diseases of the inner ear, before the perfusion, the subjects were evaluated using the brain observation sequences. After that, The Magnevist (and some studies Gadovist) was administered bolus with a concentration of 0.2 ml / kg (0,1 ml/kg Gadovist) of body weight and a rate of 5 ml per second. After delay (15 sec. or 5 sec.) the scanning session was started.

Perfusion was estimated by changing parameters - CBF, CBV, MTT.

As a result, there are no perfusion with a 15 seconds delay. I guess that we skip the time of entry of the contrast agent in the inner ear tissues (Figure 33).

a. 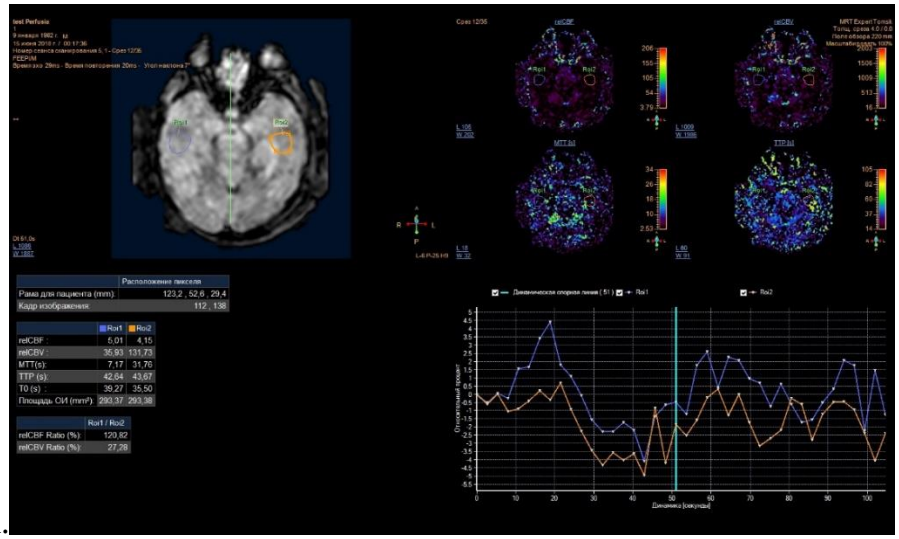

b. 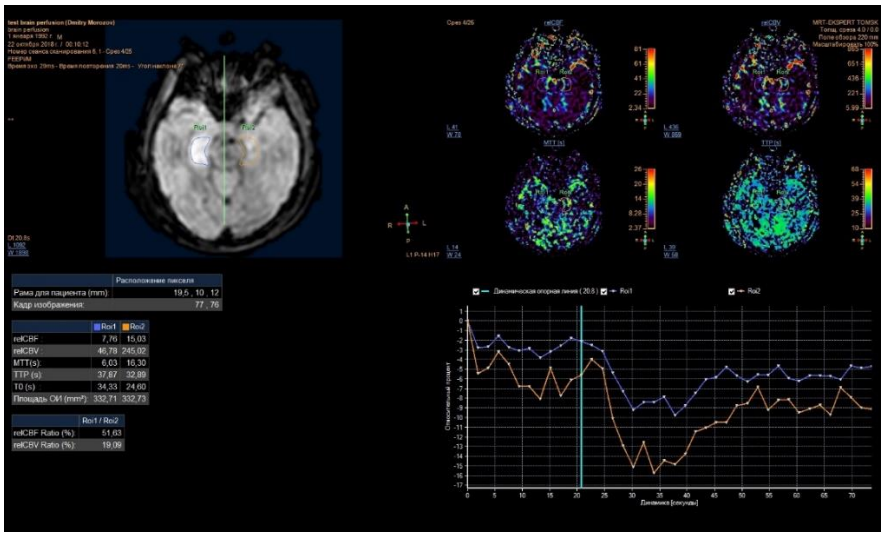

c. 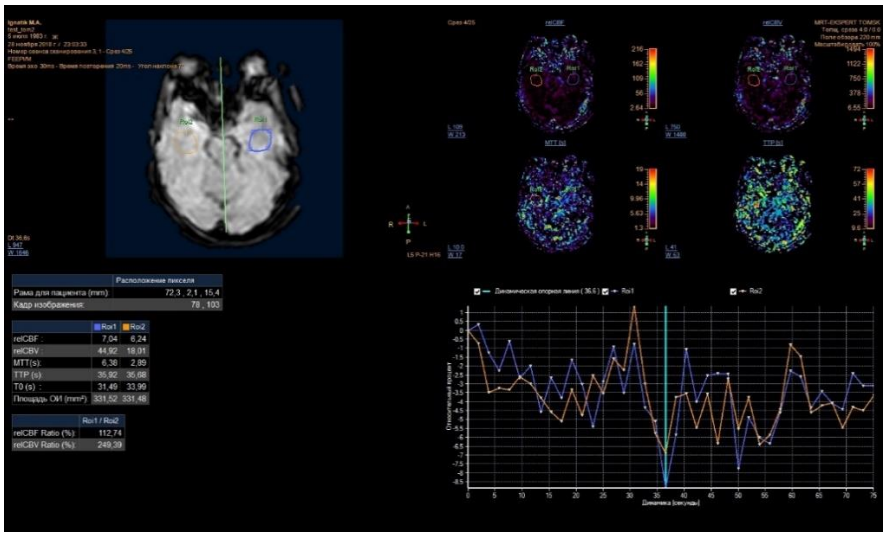

a – subject 1; b – subject 2; c. – subject 3.

Figure 33 – The perfusion with the 15 second delay.

In a 5 second delay we see the significant changes in CBF, CBV that allow to suggest perfusion detection.

Studies with the a delay of 5 seconds.

a.

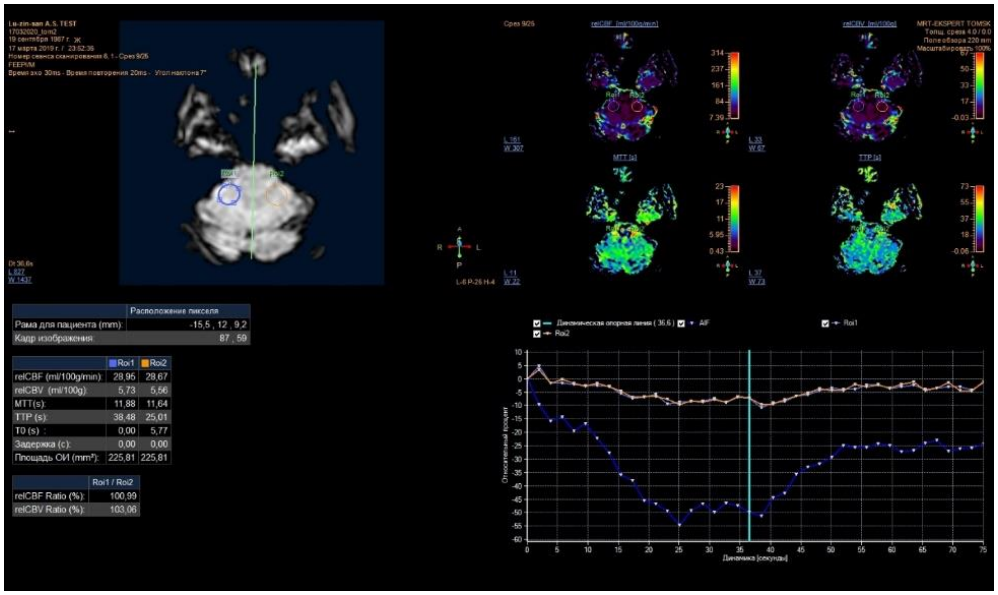

b.

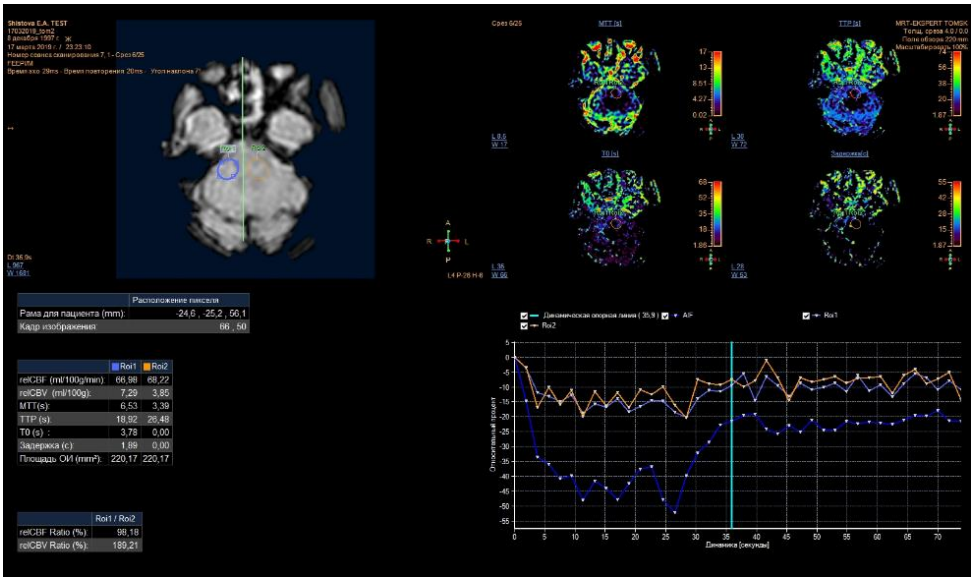

a – subject 1; b – subject 2

Figure 34 – Perfusion detection with a 5 seconds delay

CONCLUSION

The experimental part was performed in accordance with the rules of Good clinical practice (GCP) guidance. A study protocol was developed, informed patient consents were signed, the Safety Screening Form was developed. Two types of studies 22were used - from one side - daily routine studies of radiologists (using standard programs) and other side - new experimental sequences were used for obtaining high-resolution images (such as Drive and Space).

In the first steps, we used to use T1 and T2 relaxation in order to receive signal of inner ear in brain observational study. It would be the best way for physicians. Unfortunately, there is no information about inner ear. The resolution is too low and observational area is big.

After that, it needed to assess the location of vessels in brain which nourish the inner ear. We used TOF angiography, the method is based around a conventional 2D or 3D gradient echo (GRE) sequence with optional gradient-moment nulling. We did the two studies – with contrasting and without contrasting. There are no differences between two studies.

As known, the inner contain liquid. And therefore, theoretically It can be assessed using T1 and T2 fast sequence's. T1 TSE, T1 Mprage showed us the low signal from inner ear. Obviously, so a tiny anatomical structure cannot be evaluated using T1 without contrasting.

The best signal we received using T2 Space sequience on 3 Tesla Siemens magnetom MRI scanner and T2 Drive sequence on 1,5 Tesla Philips Intera MRI scanner. Drive and Space successfully came to evaluate the vestibular system. We do not see any differences in the images and correlating the risk-benefit for the patient, we believe that it is possible to investigate the anatomical structure and blood flow assessment on the 1.5 Tesla scanners. We consider that the 1,5 Tesla MRI scanner can be used for vestibular system assessment. We used the standard voxel size 0,3mmx0,3mmx0,3mm with 1mm slices. In future studies we will decrease the voxel size. Briefly writing about TR and TE, TR was about 2500 ms and TE 250 ms. The next trial will be focused on anatomical visualization of inner ear compartments and It can be done with shorter TE and reconstructing with T2-mapping.

A modified echo-planar PRESTO sequence was used to detect perfusion. Presto allows to detect the speed of passage of contrast through the vascular vessels and tissues by quickly switching gradients and obtaining multiple images. Perfusion detection is performed by comparing fast images. Due to the fact there are no literature data of blood supply (volume, speed) from the injection place to the inner ear, the study was aimed to choose the right physical parameters to detect perfusion. The Presto is a method which installed in different types MRI Scanners. This reason, this method was chosen. It's necessary time to reach the inner ear from injection place (arm vein). To

solve this task, we used the 15 sec delay and 5 sec delay before scanning. The positive results (CBV and CDF were changed) were achieved using 5 seconds delay. This parameter will be used for future studies. Next steps are the detection of perfusion using other methods – DSC, DSE, ASL and Cerebral Blood Flow, Cerebral Blood Volume of inner ear calculation. The methods such as DSC and DSE can be combine with the Presto in one study. Variability will provide accurate results.

According to the results, we obtained the anatomical structure of the vestibular system with 1.5 Tesla MRI Philips Achieva, we obtained a high-quality anatomical structure using the T2 Drive 3.0 Tesla Siemens Magnetom. According to the results of the Master's thesis, T2 Space and T2

We found that the 15 second scan delay after contrast was injected did not allow us to see the perfusion. We received positive perfusion at a 5 second delay.

To improve the quality of images, we will change the parameters TE, TE, flip angle, resolution. Cerebral blood flow will be built after determining the lower limit in healthy patients. To do this, a large number of studies will be conducted on healthy volunteers.

REFERENCES

1 A. Giesemann , E. Hofmann. Some Remarks on Imaging of the Inner Ear: Options and Limitations // Clin Neuroradiol. - 2015 - Suppl 2 - P. 197-203.

2 Tsutomu Nakashima , Shinji Naganawa , Michihiko Sone , Mitsuo Tominaga , Hideo Hayashi , Hiroshi Yamamoto, Xiuli Liu , Alfred L. Nuttall. Disorders of cochlear blood flow // Brain Research Reviews. – 2003. - Vol. 43. - P.17–28

3 Fei Tan , Constantin Bartels , Rory McConn Walsh , Our experience with 500 patients with benign paroxysmal positional vertigo: Reexploring aetiology and reevaluating MRI investigation // Aurus Nasus Larynx – 2018. – Vol. 45, Issue 2. - Pages 248-253.

4 S. Allen Counter, Sahar Nikkhou-Aski, Peter Damberg, Cecilia Engmer Berglin, and Goran Laurell, Ultra-high-field (9.4 T) MRI Analysis of Contrast Agent Transport Across the Blood–Perilymph Barrier and Intrastrial Fluid–Blood Barrier in the Mouse Inner Ear // Otology & Neurotology - 2017.

5 David S. Thylur, BA, Russell E. Jacobs, PhD, John L. Go, MD, Arthur W. Toga, PhD, John K. Niparko, Otol Neurotol. – 2017. – Vol. 38(1). - P. 133–138.

6 Nader Zakhari, Michael S. Taccone, Carlos H. Torres, Santanu Chakraborty, John Sinclair, John Woulfe, Gerard H. Jansen, Greg O. Cron, Rebecca E. Thornhill, Matthew D.F. McInnes, Thanh B Nguyen. Prospective Comparative Diagnostic Accuracy Evaluation of Dynamic Contrast-Enhanced (DCE) vs. Dynamic Susceptibility Contrast (DSC) MR Perfusion in Differentiating Tumor Recurrence From Radiation Necrosis in Treated High-Grade Gliomas // Journal of Magnetic Resonance Imaging. - 2019.

7 Zou J, Pyykkö I, Yoshida T, Gürkov R, Shi H, Li Y, et al. Milestone Research on Meniere's Disease by Visualizing Endolymphatic Hydrops Using Gadolinium-Enhanced Inner Ear MRI and the Challenges in Clinical Applications // Austin J Radiol. – 2015. – Vol. 2(6). - P. 1035

8 Jeremy Hornibrook, FRACS, and Philip Bird. A New Theory for Meniere's Disease:Detached Saccular Otoconia // Otolaryngol Head Neck Surg. – 2017. – Vol.156(2). - P. 350-352.

9 Ivanova I.V. Diagnostic Radiology in Cochlea Implant Surgery: Current Trends and Future Development (Literature Review) // Radiology – Practice - №6 – 2014. P.50-58.

10 M.N. Pakdaman, G. Ishiyama, A. Ishiyama, K.A. Peng, H.J. Kim, W.B. Pope and A.R. Sepahdari American Journal of Neuroradiology – 2016. – Vol.37(10)- P. 1903-1908

11 Paul S. Tofts. T1-weighted DCE Imaging Concepts: Modelling, Acquisition and Analysis // MAGNETOM Flash - 2010 – P.30-39.

12 Young, A., Rosengren, S., Welgampola, M. (2018). Disorders of the inner-ear balance organs and their pathways. // Handbook of Clinical Neurology, Vol. 159, P.385-401.

13 Fukushima M, Yokoi K, Iga J, Akahani S, Inohara H, Takeda N. Contralateral type of delayed endolymphatic hydrops may consist of two phenotypes based on a magnetic resonance imaging preliminary study // Acta Otolaryngol. – 2017. – Vol.137(11) – P.1153-1157.

14 American College of Radiology. // ACR Appropriateness Criteria Hearing Loss and/or Vertigo – 2018 – p.1-14.

15 J.I. Lane, R.J. Witte, B. Bolster, M.A. Bernstein, K. Johnson and J. Morris // American Journal of Neuroradiology - April 2008 – P.1436-1440.

16 Viallon M, Cuvinciuc V, Delattre B, Merlini L, Barnaure-Nachbar I, Toso-Patel S, Becker M, Lovblad KO, Haller S. State-of-the-art MRI techniques in neuroradiology: principles, pitfalls, and clinical applications. // Neuroradiology – May 2015. - Vol. 57(5) - P441-467.

17 Andrew F. Mills, Osamu Sakai, Stephan W. Anderson, Hernan Jara. Principles of Quantitative MR Imaging with Illustrated Review of Applicable Modular Pulse Diagrams. // Radio Graphics. – 2017. - Vol 37(7) – P.2083-2105.

18 Andrew F. Mills, Osamu Sakai, Stephan W. Anderson, Hernan Jara. The PRESTO technique for fMRI // Neuroimage – August 2012 - Vol. 62(2). - P. 676-681.

19 Counter SA, Nikkhou-Aski S, Damberg P, Berglin CE, Laurell G. Ultra-high-field (9.4 T) MRI Analysis of Contrast Agent Transport Across the Blood-Perilymph Barrier and Intrastrial Fluid-Blood Barrier in the Mouse Inner Ear. // Otol Neurotol. – August 2017. - Vol.38(7) - P.1052-1059.

20 Lee J, Kim ES, Lee Y, Lee K, Yoon DY, Ju YS, Lee HJ, Hong SK, Kwon MJ. Quantitative analysis of cochlear signal intensity on three-dimensional and contrast-enhanced fluid-attenuated inversion recovery images in patients with Meniere's disease: Correlation with the pure tone audiometry test. // J Neuroradiol. – April 2019 – P.5-10.

21 Fischer N, Johnson Chacko L, Glueckert R, Schrott-Fischer A. Age-Dependent Changes in the Cochlea // Gerontology. – May 2019 – p. 1-7.

22 Sung Huhn Kim, MD, Gi-Sung Nam, and Jae Young Choi. Pathophysiologic Findings in the Human Endolymphatic Sac in Endolymphatic Hydrops: Functional and Molecular Evidence // Annals of Otology, Rhinology & Laryngology 2019, Vol. 128(6S), P. 76S–83S.

23 Kovács M, Uzsaly J, Bodzai G, Harmat K, Németh A, Gerlinger I, Bakó P. Analysis of prognostic factors influencing the effectiveness of treatment in sudden sensorineural hearing loss //Orv Hetil. – 2019. - Vol. 160(18) - p687–693.

24 Kaitian Chena , Hongyan Jiangb , Ling Zongc , Xuan Wua. Side-related differences in sudden sensorineural hearing loss in children // International Journal of Pediatric Otorhinolaryngology, ovemer 2018, Volume 114, p. 5-8.

25 Tóth M, Roesch S, Grimm A, Plachtovics M, Hempel JM, Rasp G. The Role of Fissula Ante Fenestram in Unilateral Sudden Hearing Loss // Laryngoscope. – Decemer 2016. – Vol.126(12). – p. 2823-2826.

26 Chavhan GB, Babyn PS, Thomas B. Principles, techniques, and applications of T2*-based MR imaging and its special applications. // Radiographics. - 2009. – Vol.29. – p. 1433-1449.

27 Elster AD. An index system for comparative parameter weighting in MR imaging // J Comput Assist Tomogr. – 1988. - Vol.12. – p. 130-134.

28 Saloner D. An introduction to MR angiography // Radiographics. – 1995. – Vol.15. – p. 453-465.

29 Sinnaeve D. The Stejskal–Tanner equation generalized for any gradient shape—an overview of most pulse sequences measuring free diffusion // Concepts Magn Reson Part A. - 2012-Vol.40A, p.39-65

30 Pozorski V, Oh JM, Okonkwo O, Krislov S, Barzgari A, Theisen F, Sojkova J, Bendlin BB, Johnson SC, Gallagher CL. Cross-sectional and longitudinal associations between total and regional white matter hyper intensity volume and cognitive and motor function in Parkinson's disease // Neuroimage Clin. – May 2019. – Vol.23. – p.1-10.

31 Ryu K, Shin NY, Kim DH, Nam Y. Synthesizing T1 weighted MPRAGE image from multi echo GRE images via deep neural network // Magn Reson Imaging. – April 2019. – p. 725x-S0730.

32 Lea J, Pothier D. Vestibular Disorders // Adv Otorhinolaryngol. – 2019. - Vol.82, p.67–76.

APPENDIX A

Safety Screening Form.

Safety screening form MRI

Version 1

I have understood the following questions and answered honestly:

- Do you have an active implant? ☐ Yes ☐ No
  (pacemaker, neurostimulator, insulin pump, ossicle prosthesis, or residual leads)

- Do you have any other foreign objects in your body, except dental fillings or crowns? ☐ Yes ☐ No
  (e. g. clips on blood vessels, metal splinters in the eye or body as consequence of shooting/accident/metal worker, orthopedic implants, braces, metal wire behind the teeth, mechanical contraception spiral)

  If yes, what kind of foreign object?

- Have you had surgery to your brain, head? ☐ Yes ☐ No

- Do you suffer from epilepsy? ☐ Yes ☐ No

- Do you suffer from any known heart rhythm disorder? ☐
  Yes ☐ No

- Do you have circulatory problems? ☐ Yes ☐ No

- Are you diabetic? ☐ Yes ☐ No

- Do you suffer from claustrophobia? ☐ Yes ☐ No

- Are you pregnant or do think that you might be? ☐ Yes ☐ No

- Do you wear jewelry/piercings that cannot be taken of? ☐ Yes ☐ No

- Do you have tattoos or permanent eye make-up? ☐ Yes ☐ No

  If yes, describe what and where:

- Are you using medical plasters (e.g. nicotine) that cannot be taken of? ☐ Yes ☐ No
- Do you have any drug allergic? ☐ Yes ☐ No

  If yes, which one:
- Do you have any renal disease? ☐ Yes ☐ No

  If yes, describe what kind of disease:

I have been informed to satisfaction concerning the MRI safety. I had the possibility to ask questions concerning MRI safety. All my questions are answered to my satisfaction. I am aware that this form is kept in accordance with the privacy statements.

I agree with being scanned:

Last name: Today's date:

First name: Date of birth:

Middle name (if any): Height (cm):

Weight (kg):

Signature:

To be filled out by the certified user (all fields are obligated)

Name: MR System: Project number:

I declare that the person mentioned above has been informed orally and in writing about the MRI scan and has given their informed consent about the project mentioned above. I also declare that premature termination of participation by the person mentioned above will be of no influence on the care he or she will receive.

Function:

APPENDIX B

Parameters of the scans session.

\\USER\Bianca Linssen\Cochlea\cochlea\localizer
TA: 0:12 PM: REF Voxel size: 0.5×0.5×7.0 mmPAT: Off Rel. SNR: 1.00 : fl

Properties

Prio recon	On
Load images to viewer	On
Inline movie	Off
Auto store images	On
Load images to stamp segments	On
Load images to graphic segments	On
Auto open inline display	Off
Auto close inline display	Off
Start measurement without further preparation	On
Wait for user to start	Off
Start measurements	Single measurement

Routine

Slice group	1
Slices	1
Dist. factor	20 %
Position	L0.0 A20.0 H0.0 mm
Orientation	Sagittal
Phase enc. dir.	A >> P
Slice group	2
Slices	1
Dist. factor	20 %
Position	L0.0 A20.0 H0.0 mm
Orientation	Transversal
Phase enc. dir.	A >> P
Slice group	3
Slices	1
Dist. factor	20 %
Position	L0.0 A20.0 H0.0 mm
Orientation	Coronal
Phase enc. dir.	R >> L
AutoAlign	---
Phase oversampling	0 %
FoV read	250 mm
FoV phase	100.0 %
Slice thickness	7.0 mm
TR	7.5 ms
TE	3.69 ms
Averages	2
Concatenations	3
Filter	Prescan Normalize, Elliptical filter
Coil elements	HE1-4

Contrast - Common

TR	7.5 ms
TE	3.69 ms
TD	0 ms
MTC	Off
Magn. preparation	None
Flip angle	20 deg
Fat suppr.	None
Water suppr.	None
SWI	Off

Contrast - Dynamic

Averages	2
Averaging mode	Short term
Reconstruction	Magnitude
Measurements	1

Contrast - Dynamic

Multiple series	Each measurement

Resolution - Common

FoV read	250 mm
FoV phase	100.0 %
Slice thickness	7.0 mm
Base resolution	256
Phase resolution	91 %
Phase partial Fourier	Off
Interpolation	On

Resolution - iPAT

PAT mode	None

Resolution - Filter Image

Image Filter	Off
Distortion Corr.	Off
Prescan Normalize	On
Unfiltered images	Off
Normalize	Off
B1 filter	Off

Resolution - Filter Rawdata

Raw filter	Off
Elliptical filter	On

Geometry - Common

Slice group	1
Slices	1
Dist. factor	20 %
Position	L0.0 A20.0 H0.0 mm
Orientation	Sagittal
Phase enc. dir.	A >> P
Slice group	2
Slices	1
Dist. factor	20 %
Position	L0.0 A20.0 H0.0 mm
Orientation	Transversal
Phase enc. dir.	A >> P
Slice group	3
Slices	1
Dist. factor	20 %
Position	L0.0 A20.0 H0.0 mm
Orientation	Coronal
Phase enc. dir.	R >> L
FoV read	250 mm
FoV phase	100.0 %
Slice thickness	7.0 mm
TR	7.5 ms
Multi-slice mode	Sequential
Series	Interleaved
Concatenations	3

Geometry - AutoAlign

Slice group	1
Position	L0.0 A20.0 H0.0 mm
Orientation	Sagittal
Phase enc. dir.	A >> P
Slice group	2
Position	L0.0 A20.0 H0.0 mm

Geometry - AutoAlign

Orientation	Transversal
Phase enc. dir.	A >> P
Slice group	3
Position	L0.0 A20.0 H0.0 mm
Orientation	Coronal
Phase enc. dir.	R >> L
AutoAlign	---
Initial Position	L0.0 A20.0 H0.0
L	0.0 mm
A	20.0 mm
H	0.0 mm
Initial Rotation	0.00 deg
Initial Orientation	Sagittal

Geometry - Saturation

Saturation mode	Standard
Fat suppr.	None
Water suppr.	None
Special sat.	None

System - Miscellaneous

Positioning mode	REF
Table position	H
Table position	0 mm
MSMA	S - C - T
Sagittal	R >> L
Coronal	A >> P
Transversal	F >> H
Coil Combine Mode	Adaptive Combine
Save uncombined	Off
Matrix Optimization	Off
AutoAlign	---
Coil Select Mode	Off - AutoCoilSelect

System - Adjustments

B0 Shim mode	Tune up
B1 Shim mode	TrueForm
Adjust with body coil	Off
Confirm freq. adjustment	Off
Assume Dominant Fat	Off
Assume Silicone	Off
Adjustment Tolerance	Auto

System - Adjust Volume

Position	Isocenter
Orientation	Transversal
Rotation	0.00 deg
A >> P	263 mm
R >> L	350 mm
F >> H	350 mm
Reset	Off

System - pTx Volumes

B1 Shim mode	TrueForm
Excitation	Slice-sel.

System - Tx/Rx

Frequency 1H	123.250874 MHz
Correction factor	1
Gain	High
Img. Scale Cor.	1.000
Reset	Off
? Ref. amplitude 1H	0.000 V

Physio - Signal1

1st Signal Mode	None
TR	7.5 ms
Concatenations	3
Segments	1

Physio - Cardiac

Magn. preparation	None
Fat suppr.	None
Dark blood	Off
FoV read	250 mm
FoV phase	100.0 %
Phase resolution	91 %

Physio - PACE

Resp. control	Off
Concatenations	3

Inline - Common

Subtract	Off
Measurements	1
StdDev	Off
Liver registration	Off
Save original images	On

Inline - MIP

MIP-Sag	Off
MIP-Cor	Off
MIP-Tra	Off
MIP-Time	Off
Save original images	On

Inline - Soft Tissue

Wash - In	Off
Wash - Out	Off
TTP	Off
PEI	Off
MIP - time	Off
Measurements	1

Inline - Composing

Distortion Corr.	Off

Inline - MapIt

Save original images	On
MapIt	None
Flip angle	20 deg
Measurements	1
Contrasts	1
TR	7.5 ms
TE	3.69 ms

Sequence - Part 1

Introduction	On
Dimension	2D
Phase stabilisation	Off
Asymmetric echo	Allowed
Contrasts	1
Flow comp.	No
Multi-slice mode	Sequential
Bandwidth	320 Hz/Px

Sequence - Part 2

Segments	1

Sequence - Part 2

Acoustic noise reduction	None
RF pulse type	Fast
Gradient mode	Fast
Excitation	Slice-sel.
RF spoiling	On

Sequence - Assistant

Mode	Off
Allowed delay	0 s

\\USER\Bianca Linssen\Cochlea\cochlea\t1_tse_r_tra_2mm
TA: 2:19 PM: REF Voxel size: 0.3×0.3×3.0 mmPAT: 2 Rel. SNR: 1.00 : tse_ns

Properties

Pno recon	Off
Load images to viewer	On
Inline movie	Off
Auto store images	On
Load images to stamp segments	Off
Load images to graphic segments	Off
Auto open inline display	Off
Auto close inline display	Off
Start measurement without further preparation	Off
Wait for user to start	Off
Start measurements	Single measurement

Routine

Slice group	1
Slices	14
Dist. factor	10 %
Position	Isocenter
Orientation	Transversal
Phase enc. dir.	R >> L
AutoAlign	---
Phase oversampling	30 %
FoV read	160 mm
FoV phase	100.0 %
Slice thickness	3.0 mm
TR	650.0 ms
TE	8 ms
Averages	3
Concatenations	1
Filter	Prescan Normalize, Elliptical filter
Coil elements	HC1-7

Contrast - Common

TR	650.0 ms
TE	8 ms
MTC	Off
Magn. preparation	None
Flipangle	120 deg
Fat suppr.	None
Water suppr.	None
Restore magn.	Off

Contrast - Dynamic

Averages	3
Averaging mode	Long term
Reconstruction	Magnitude
Measurements	1
Multiple series	Each measurement

Resolution - Common

FoV read	160 mm
FoV phase	100.0 %
Slice thickness	3.0 mm
Base resolution	320
Phase resolution	100 %
Phase partial Fourier	Off
Trajectory	Cartesian
Interpolation	On

Resolution - iPAT

PAT mode	GRAPPA
Accel. factor PE	2
Ref. lines PE	32
Reference scan mode	Self-calibration

Resolution - Filter Image

Image Filter	Off
Distortion Corr.	Off
Prescan Normalize	On
Unfiltered images	Off
Normalize	Off
B1 filter	Off

Resolution - Filter Rawdata

Raw filter	Off
Elliptical filter	On

Geometry - Common

Slice group	1
Slices	14
Dist. factor	10 %
Position	Isocenter
Orientation	Transversal
Phase enc. dir.	R >> L
FoV read	160 mm
FoV phase	100.0 %
Slice thickness	3.0 mm
TR	650.0 ms
Multi-slice mode	Interleaved
Series	Interleaved
Concatenations	1

Geometry - AutoAlign

Slice group	1
Position	Isocenter
Orientation	Transversal
Phase enc. dir.	R >> L
AutoAlign	---
Initial Position	Isocenter
L	0.0 mm
P	0.0 mm
H	0.0 mm
Initial Rotation	90.00 deg
Initial Orientation	Transversal

Geometry - Saturation

Sat. region	1
Thickness	60 mm
Position	R0.1 P48.1 H17.3 mm
Orientation	Transversal
Shape	Standard
Water suppr.	None
Restore magn.	Off
Special sat.	Parallel F
Gap	7 mm
Thickness	60 mm

Geometry - Navigator

System - Miscellaneous

Positioning mode	REF
Table position	H
Table position	0 mm
MSMA	S - C - T
Sagittal	R >> L
Coronal	A >> P
Transversal	F >> H
Coil Combine Mode	Adaptive Combine
Save uncombined	Off
Matrix Optimization	Off
AutoAlign	---
Coil Select Mode	Off - AutoCoilSelect

System - Adjustments

B0 Shim mode	Tune up
B1 Shim mode	TrueForm
Adjust with body coil	Off
Confirm freq. adjustment	Off
Assume Dominant Fat	Off
Assume Silicone	Off
Adjustment Tolerance	Auto

System - Adjust Volume

Position	Isocenter
Orientation	Transversal
Rotation	0.00 deg
A >> P	269 mm
R >> L	380 mm
F >> H	380 mm
Reset	Off

System - pTx Volumes

B1 Shim mode	TrueForm

System - Tx/Rx

Frequency 1H	123.250874 MHz
Correction factor	1
Gain	High
Img. Scale Cor.	1.000
Reset	Off
? Ref. amplitude 1H	0.000 V

Physio - Signal1

1st Signal Mode	None
TR	650.0 ms
Concatenations	1

Physio - Cardiac

Magn. preparation	None
Fat suppr.	None
Dark blood	Off
FoV read	160 mm
FoV phase	100.0 %
Phase resolution	100 %
Trajectory	Cartesian

Physio - PACE

Resp. control	Off
Concatenations	1

Inline - Common

Subtract	Off
Measurements	1

Inline - Common

StdDev	Off
Save original images	On

Inline - MIP

MIP-Sag	Off
MIP-Cor	Off
MIP-Tra	Off
MIP-Time	Off
Save original images	On

Inline - Composing

Distortion Corr.	Off

Sequence - Part 1

Introduction	On
Dimension	2D
Compensate T2 decay	Off
Reduce Motion Sens.	On
Contrasts	1
Flow comp.	Slice
Multi-slice mode	Interleaved
Free echo spacing	Off
Echo spacing	7.95 ms
Bandwidth	363 Hz/Px

Sequence - Part 2

Define	Turbo factor
Echo trains per slice	70
Phase correction	Automatic
Acoustic noise reduction	None
RF pulse type	Fast
Gradient mode	Performance
Hyperecho	Off
WAIP	Off
Red. EC sensitivity	Off
Turbo factor	3

Sequence - Assistant

Mode	Min flip angle
Min flip angle	130 deg
Allowed delay	60 s

\\USER\Bianca Linssen\Cochlea\cochlea\t2_space_tra_0.2x0.2x0.5ip
TA: 8:16 PM: REF Voxel size: 0.2×0.2×0.5 mmPAT: 2 Rel. SNR: 1.00 : spcR

Properties

Prio recon	Off
Load images to viewer	On
Inline movie	Off
Auto store images	On
Load images to stamp segments	Off
Load images to graphic segments	Off
Auto open inline display	Off
Auto close inline display	Off
Start measurement without further preparation	Off
Wait for user to start	Off
Start measurements	Single measurement

Routine

Slab group	1
Slabs	1
Position	Isocenter
Orientation	Transversal
Phase enc. dir.	R >> L
AutoAlign	---
Phase oversampling	10 %
Slice oversampling	12.5 %
Slices per slab	128
FoV read	150 mm
FoV phase	100.0 %
Slice thickness	0.50 mm
TR	2000 ms
TE	279 ms
Averages	1.4
Concatenations	1
Filter	Raw filter, Prescan Normalize
Coil elements	HC1-7

Contrast - Common

TR	2000 ms
TE	279 ms
MTC	Off
Magn. preparation	None
Flip angle	120 deg
Fat suppr.	None
Blood suppr.	Off
Restore magn.	On

Contrast - Dynamic

Averages	1.4
Reconstruction	Magnitude
Measurements	1
Multiple series	Each measurement

Resolution - Common

FoV read	150 mm
FoV phase	100.0 %
Slice thickness	0.50 mm
Base resolution	320
Phase resolution	100 %
Slice resolution	50 %
Phase partial Fourier	Allowed
Slice partial Fourier	Off
Interpolation	On

Resolution - iPAT

PAT mode	GRAPPA
Accel. factor PE	2
Ref. lines PE	24
Accel. factor 3D	1
Reference scan mode	Integrated

Resolution - Filter Image

Image Filter	Off
Distortion Corr.	Off
Prescan Normalize	On
Unfiltered images	Off
Normalize	Off
B1 filter	Off

Resolution - Filter Rawdata

Raw filter	On
Elliptical filter	Off

Geometry - Common

Slab group	1
Slabs	1
Position	Isocenter
Orientation	Transversal
Phase enc. dir.	R >> L
Slice oversampling	12.5 %
Slices per slab	128
FoV read	150 mm
FoV phase	100.0 %
Slice thickness	0.50 mm
TR	2000 ms
Series	Ascending
Concatenations	1

Geometry - AutoAlign

Slab group	1
Position	Isocenter
Orientation	Transversal
Phase enc. dir.	R >> L
AutoAlign	---
Initial Position	Isocenter
L	0.0 mm
P	0.0 mm
H	0.0 mm
Initial Rotation	90.00 deg
Initial Orientation	Transversal

Geometry - Saturation

Fat suppr.	None
Restore magn.	On
Special sat.	None

Geometry - Navigator

System - Miscellaneous

Positioning mode	REF
Table position	H
Table position	0 mm
MSMA	S - C - T
Sagittal	R >> L
Coronal	A >> P

System - Miscellaneous

Transversal	F >> H
Coil Combine Mode	Adaptive Combine
Save uncombined	Off
Matrix Optimization	Off
AutoAlign	---
Coil Select Mode	Off - AutoCoilSelect

System - Adjustments

B0 Shim mode	Tune up
B1 Shim mode	TrueForm
Adjust with body coil	Off
Confirm freq. adjustment	Off
Assume Dominant Fat	Off
Assume Silicone	Off
Adjustment Tolerance	Auto

System - Adjust Volume

Position	Isocenter
Orientation	Transversal
Rotation	0.00 deg
A >> P	260 mm
R >> L	300 mm
F >> H	300 mm
Reset	Off

System - pTx Volumes

B1 Shim mode	TrueForm
Excitation	Slab-sel.

System - Tx/Rx

Frequency 1H	123.250874 MHz
Correction factor	1
Gain	High
Img. Scale Cor.	1.000
Reset	Off
? Ref. amplitude 1H	0.000 V

Physio - Signal1

1st Signal/Mode	None
Trigger delay	0 ms
TR	2000 ms
Concatenations	1

Physio - Cardiac

Magn. preparation	None
Fat suppr.	None
Dark blood	Off
FoV read	180 mm
FoV phase	100.0 %
Phase resolution	100 %

Physio - PACE

Resp. control	Off
Concatenations	1

Inline - Common

Subtract	Off
Measurements	1
StdDev	Off
Save original images	On

Inline - MIP

MIP-Sag	Off

Inline - MIP

MIP-Cor	Off
MIP-Tra	Off
MIP-Time	Off
Save original images	On

Inline - Composing

Distortion Corr.	Off

Sequence - Part 1

Introduction	On
Dimension	3D
Elliptical scanning	Off
Reordering	Linear
Flow comp.	No
Echo spacing	6.65 ms
Adiabatic-mode	Off
Bandwidth	289 Hz/Px

Sequence - Part 2

Echo train duration	525 ms
RF pulse type	Normal
Gradient mode	Fast
Excitation	Slab-sel.
Flip angle mode	Constant
Turbo factor	77

Sequence - Assistant

Allowed delay	30 s

\\USER\Bianca Linssen\Cochlea\cochlea\t1_mprage_tra_p2_iso_gado
TA: 5:38 PM: REF Voxel size: 0.9×0.9×1.0 mmPAT: 2 Rel. SNR: 1.00 : tfl

Properties

Prio recon	Off
Load images to viewer	On
Inline movie	Off
Auto store images	On
Load images to stamp segments	Off
Load images to graphic segments	Off
Auto open inline display	Off
Auto close inline display	Off
Start measurement without further preparation	Off
Wait for user to start	Off
Start measurements	Single measurement

Routine

Slab group	1
Slabs	1
Dist. factor	50 %
Position	Isocenter
Orientation	Transversal
Phase enc. dir.	R >> L
AutoAlign	---
Phase oversampling	10 %
Slice oversampling	27.3 %
Slices per slab	176
FoV read	230 mm
FoV phase	100.0 %
Slice thickness	1.00 mm
TR	2200.0 ms
TE	2.48 ms
Averages	1
Concatenations	1
Filter	Prescan Normalize, Image Filter
Coil elements	HE1-4

Contrast - Common

TR	2200.0 ms
TE	2.48 ms
Magn. preparation	Non sel. IR
TI	900 ms
Flip angle	8 deg
Fat suppr.	None
Water suppr.	None

Contrast - Dynamic

Averages	1
Averaging mode	Long term
Reconstruction	Magnitude
Measurements	1
Multiple series	Each measurement

Resolution - Common

FoV read	230 mm
FoV phase	100.0 %
Slice thickness	1.00 mm
Base resolution	256
Phase resolution	100 %
Slice resolution	100 %
Phase partial Fourier	Off
Slice partial Fourier	Off

Resolution - Common

Interpolation	Off

Resolution - iPAT

PAT mode	GRAPPA
Accel. factor PE	2
Ref. lines PE	24
Accel. factor 3D	1
Reference scan mode	Integrated

Resolution - Filter Image

Image Filter	On
! Intensity	Medium
Edge Enhancement	3
Smoothing	2
Unfiltered Images	Off
Distortion Corr.	Off
Prescan Normalize	On
Unfiltered Images	Off
Normalize	Off
B1 filter	Off

Resolution - Filter Rawdata

Raw filter	Off
Elliptical filter	Off

Geometry - Common

Slab group	1
Slabs	1
Dist. factor	50 %
Position	Isocenter
Orientation	Transversal
Phase enc. dir.	R >> L
Slice oversampling	27.3 %
Slices per slab	176
FoV read	230 mm
FoV phase	100.0 %
Slice thickness	1.00 mm
TR	2200.0 ms
Multi-slice mode	Single shot
Series	Ascending
Concatenations	1

Geometry - AutoAlign

Slab group	1
Position	Isocenter
Orientation	Transversal
Phase enc. dir.	R >> L
AutoAlign	---
Initial Position	Isocenter
L	0.0 mm
P	0.0 mm
H	0.0 mm
Initial Rotation	90.00 deg
Initial Orientation	Transversal

Geometry - Navigator

System - Miscellaneous

Positioning mode	REF
Table position	H

System - Miscellaneous

Table position	0 mm
MSMA	S - C - T
Sagittal	R >> L
Coronal	A >> P
Transversal	F >> H
Coil Combine Mode	Adaptive Combine
Save uncombined	Off
Matrix Optimization	Off
AutoAlign	---
Coil Select Mode	Off - AutoCoilSelect

System - Adjustments

B0 Shim mode	Tune up
B1 Shim mode	TrueForm
Adjust with body coil	Off
Confirm freq. adjustment	Off
Assume Dominant Fat	Off
Assume Silicone	Off
Adjustment Tolerance	Auto

System - Adjust Volume

Position	Isocenter
Orientation	Transversal
Rotation	0.00 deg
A >> P	253 mm
R >> L	350 mm
F >> H	350 mm
Reset	Off

System - pTx Volumes

B1 Shim mode	TrueForm
Excitation	Slab-sel.

System - Tx/Rx

Frequency 1H	123.250874 MHz
Correction factor	1
Gain	Low
Img. Scale Cor.	1.000
Reset	Off
? Ref. amplitude 1H	0.000 V

Physio - Signal1

1st Signal/Mode	None
TR	2200.0 ms
Concatenations	1

Physio - Cardiac

Magn. preparation	Non sel. IR
TI	900 ms
Fat suppr.	None
Dark blood	Off
FoV read	230 mm
FoV phase	100.0 %
Phase resolution	100 %

Physio - PACE

Resp. control	Off
Concatenations	1

Inline - Common

Subtract	Off
Measurements	1
StdDev	Off

Inline - Common

Save original images	On

Inline - MIP

MIP-Sag	Off
MIP-Cor	Off
MIP-Tra	Off
MIP-Time	Off
Save original images	On

Inline - Composing

Distortion Corr.	Off

Inline - MapIt

Save original images	On
MapIt	None
Flip angle	8 deg
Measurements	1
TR	2200.0 ms
TE	2.48 ms

Sequence - Part 1

Introduction	On
Dimension	3D
Elliptical scanning	Off
Reordering	Linear
Asymmetric echo	Allowed
Flow comp.	No
Multi-slice mode	Single shot
Echo spacing	7.3 ms
Bandwidth	250 Hz/Px

Sequence - Part 2

RF pulse type	Fast
Gradient mode	Normal
Excitation	Slab-sel.
RF spoiling	On
Incr. Gradient spoiling	On
Turbo factor	224

Sequence - Assistant

Mode	Off

Краткий отчет

ПОЛУЧИТЬ ПОЛНЫЙ ОТЧЕТ

ВЕРСИЯ ДЛЯ ПЕЧАТИ | ЭКСПОРТ | ИСТОРИЯ ОТЧЕТОВ | РУКОВОДСТВО | ВЫЙТИ В КАБИНЕТ

ВР

ПРОВЕРЕНО: 24.06.2019 12:05:46

№	Доля в отчете	Доля в тексте	Источник	Актуальна на	Модуль поиска	Блоков в отчете	Блоков в тексте
[01]	8,61%	8,69%	State-of-the-art MRI techniques in neurora...	06 Сен 2018	Модуль поиска Интернет	88	89
[02]	3,61%	3,73%	State of the Art: 3T Imaging of the Membra...	04 Сен 2018	Модуль поиска Интернет	50	58
[03]	1,17%	1,17%	Diffusion MRI (1/2)	13 Мар 2015	Модуль поиска Интернет	13	13

ЗАИМСТВОВАНИЯ
16,35%

ЦИТИРОВАНИЯ
0%

ОРИГИНАЛЬНОСТЬ
83,65%

ИСТОЧНИКОВ: 20

ЕЩЕ НАЙДЕНО ИСТОЧНИКОВ: 17

ЗАИМСТВОВАНИЯ: 2,95%